

doi: 10.12029/gc20210209

王召林,孟贵祥,汤贺军,袁璐璐,杨竹森,肖艳东. 2021. 新疆东准噶尔扎河坝橄榄岩单斜辉石、铬尖晶石地球化学特征及铬铁矿成矿作用[J]. 中国地质, 48(2): 477–494.

Wang Zhaolin, Meng Guixiang, Tang Hejun, Yuan Lulu, Yang Zhusen, Xiao Yandong. 2021. Geochemistry of clinopyroxene and chrome spinel in the Zhaheba peridotite, Eastern Junggar, Xinjiang, China and its chromitite metallogenesis[J]. Geology in China, 48(2): 477–494(in Chinese with English abstract).

新疆东准噶尔扎河坝橄榄岩单斜辉石、铬尖晶石地球化学特征及铬铁矿成矿作用

王召林^{1,2}, 孟贵祥^{1,2}, 汤贺军^{1,2}, 袁璐璐^{1,2}, 杨竹森³, 肖艳东⁴

(1. 中国地质科学院, 北京 100037; 2. 中国地质调查局 中国地质科学院 地球深部探测中心, 北京 100037; 3. 中国地质科学院 矿产资源研究所, 北京 100037; 4. 新疆维吾尔自治区地质调查院, 新疆 乌鲁木齐 830000)

提要:扎河坝蛇绿岩是东准噶尔地区一条重要的蛇绿岩带, 主要由橄榄岩、层状辉长岩、玄武岩、斜长花岗岩、硅质岩等组成。其中橄榄岩主要由方辉辉橄榄岩(方辉橄榄岩)、二辉橄榄岩和少量纯橄榄岩组成。二辉橄榄岩中的单斜辉石 Cr_2O_3 平均 1.11 %, Al_2O_3 平均 4.77 %, MgO 平均 16.99 %, CaO 平均 21.84 %, SiO_2 平均 50.00 %; 铬尖晶石副矿物具有较低的 Cr_2O_3 (平均 40.35 %)、 $\text{Cr}^{\#}$ (平均 0.53) 和更高的 Al_2O_3 (平均 24.10 %), MgO (平均 13.23 %) 和 $\text{Mg}^{\#}$ (0.62) 含量, 属高 Al 型, 橄榄岩形成于扎河坝洋扩张时期(MOR 环境); 块状铬铁矿铬尖晶石各元素含量变化较小: Cr_2O_3 平均 55.45 %, Al_2O_3 平均 10.88 %, MgO 平均 11.98 % 和 $\text{Mg}^{\#}$ 为 0.60, 属 SSZ 背景高 Cr 型铬铁矿。二辉橄榄岩单斜辉石具有典型的熔融残余结构和熔-岩反应结构, 斜方辉石保留绢石化假晶和部分未蚀变的辉石残余体(主要是顽火辉石), 铬尖晶石副矿物具有熔蚀特征。单斜辉石的熔融残余结构是含铬矿物熔融、释放铬的一种表现, 是橄榄岩部分熔融程度升高, 向更富镁方向演化的结构标志, 但可能对富 Cr 型铬铁矿的形成贡献有限。橄榄岩存在熔-岩反应新生的单斜辉石、橄榄石及结构标志。熔-岩反应过程中流体、挥发分的作用不可忽视。文章还探讨了铬铁矿 $\text{Cr}^{\#}$ 、 $\text{Mg}^{\#}$ 和 Al_2O_3 含量差异与蛇绿岩形成的构造背景关系及影响因素。卡拉麦里洋壳俯冲和地幔对流循环使扎河坝早期形成于 MOR 环境的富 Al 铬尖晶石富集, 形成高 Cr 块状铬铁矿。

关 键 词:高 Cr 铬铁矿; 铬尖晶石; 部分熔融; 熔-岩反应; 矿产勘查工程; 扎河坝蛇绿岩; 新疆

中图分类号: P618.33 文献标志码: A 文章编号: 1000-3657(2021)02-0477-18

Geochemistry of clinopyroxene and chrome spinel in the Zhaheba peridotite, Eastern Junggar, Xinjiang, China and its chromitite metallogenesis

WANG Zhaolin^{1,2}, MENG Guixiang^{1,2}, TANG Hejun^{1,2},
YUAN Lulu^{1,2}, YANG Zhusen³, XIAO Yandong⁴

(1. Chinese Academy of Geological Sciences, Beijing, 100037, China; 2. SinoProbe Center, Chinese Academy of Geological Sciences and China Geological Survey, Beijing, 100037, China; 3. Institute of Mineral Resources, Chinese Academy of Geological Sciences, Beijing, 100037, China; 4. Geological Research Academy of Xinjiang, Urumqi, 830000, Xinjiang, China)

收稿日期: 2019-12-04; 改回日期: 2020-02-18

基金项目: 中国地质调查局项目(DD20190071)和中国地质科学院基本科研业务费项目(JKY201908-01)联合资助。

作者简介: 王召林,男,1978年生,博士,教授级高级工程师,主要从事金属矿产勘查、研究工作; E-mail: geology231@126.com。

Abstract: Zhaheba ophiolite is a significant ophiolite complex in Eastern Junggar, consisting mainly of peridotite, basalt, layered gabbro, plagiogranite and chert. Among them, the peridotite is mainly composed of harzburgite, herzolite, and minor dunite. The average contents of clinopyroxene in herzolite are Cr_2O_3 1.11 %, Al_2O_3 4.77 %, MgO 16.99 %, CaO 21.84 %, SiO_2 50.00 %, and the accessory mineral chromium spinel falling within the high-Al types has lower average contents Cr_2O_3 40.35 %, $\text{Cr}^{\#}$ 0.53 but higher Al_2O_3 24.10 %, MgO 13.23 % and $\text{Mg}^{\#}(0.62)$, which indicate that it was formed during the extension of Zhaheba ocean in MOR environment. While the element contents of chrome spinels in massive chromites changes little with average contents of Cr_2O_3 55.45 %, Al_2O_3 10.88 %, MgO 11.98 % and $\text{Mg}^{\#}$ 0.60, which fall in high-Cr type fields and belong to SSZ type of chromites. Clinopyroxenes in herzolite is characterized by typical structures of melted residue and melt-rock reaction, and orthopyroxene in harzburgite kept bastitic pseudomorphs and unaltered enstatites, but chrome spinel accessory minerals show corrosion features. The melting residual structure of monocline is a manifestation of the melting and chromium release of chromium-bearing minerals, and also a structural indicator of the partial melting degree of peridotite increasing and the evolution towards more magnesium rich direction, which may have limited contribution to the formation of Cr-rich chromite. The peridotite contains monoclinopyroxene, olivine and textures newly generated from melt-rock reaction. The role of fluid and volatiles in the melt-rock reaction cannot be ignored. Based on the above studies, the relationship among the content differences of $\text{Cr}^{\#}$, $\text{Mg}^{\#}$ and Al_2O_3 of chromite and tectonic settings of ophiolite, and its influence factors are discussed. It is concluded that mantle convection and subduction of Kalamaili ocean led to the enrichment of the high-Al chrome spinels in MOR environment and forming of massive chromites.

Key words: high Cr chromites; chrome spinel; partial melting; melt-rock reaction; mineral exploration engineering; Zhaheba ophiolite; Xinjiang

About the first author: WANG Zhaolin, male, born in 1978, senior engineer, engaged in metal mineral exploration and research; E-mail: geology231@126.com.

Fund support: Supported by the project of China Geological Survey (No. DD20190071) and scientific research project of Chinese Academy of Geological Sciences (No. JKY201908-01).

1 引言

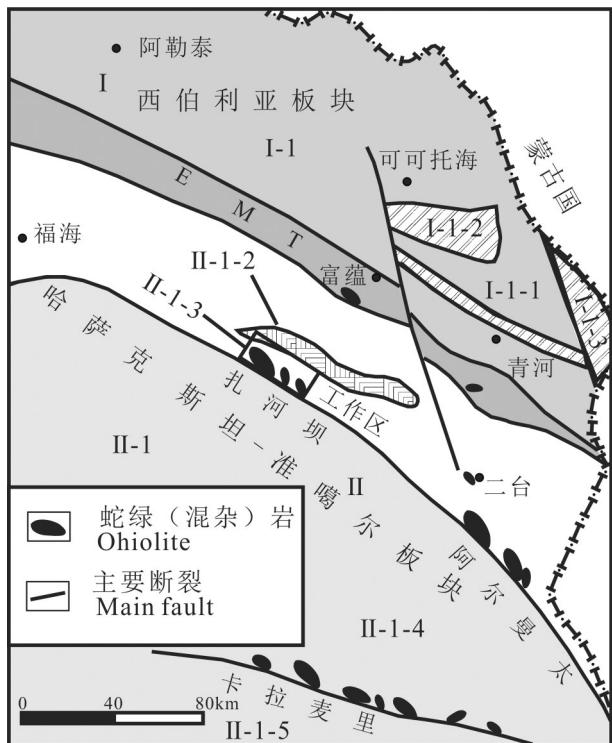
蛇绿岩带内橄榄岩中存在的铬尖晶石对橄榄岩形成时的地幔环境具有重要指示意义(Barnes and Roeder, 2001),其系列地球化学指标能够反映形成铬铁矿的岩浆的熔融程度、成分、氧逸度和构造背景等(Dick and Bullen, 1984; Pearce et al., 2000; Kamenetsky et al., 2001; Trevor et al., 2008),是判别铬铁矿铬来源与富集机制、成因类型的关键因素。大多情况下洋中脊或弧后盆地背景中形成MORB型铬铁矿尖晶石具有高Al-低Cr($\text{Cr}^{\#}<60$)特征,而俯冲带背景形成SSZ型铬铁矿其尖晶石表现富Cr现象($\text{Cr}^{\#}>60$)(Zhou and Robinson, 1994; Uysal et al., 2005, 2009; Akmaz et al., 2014; Ahmed and Abdelmonem, 2015; Erdi et al., 2017)。然而,受洋壳俯冲、蛇绿岩就位和碰撞造山作用等影响,尖晶石组成特征与构造背景的对应关系并不完全吻合(Zhou et al., 2005; Rollinson and Adetunji, 2013),而是两种特征的铬铁矿共存于同一个蛇绿岩带内,给研究蛇绿岩型铬铁矿的成因带来很大困难。

部分熔融程度与地幔橄榄岩类型、矿物成分变化的关系如何?富Al的尖晶石副矿物和单斜辉石是如何转变为富Cr的块状铬铁矿的?

为回答上述问题,本次工作对扎河坝橄榄岩进行了典型剖面测制和取样工作,在详细的室内岩相观察和电子探针工作的基础上,探讨橄榄岩部分熔融过程中辉石熔融、含铬矿物溶解及熔-岩反应用于铬铁矿形成的贡献。

2 区域地质特征

东准噶尔地区发育两条蛇绿岩带:扎河坝—阿尔曼泰蛇绿岩带和卡拉麦里蛇绿岩带,这两条蛇绿岩带先后记录了古亚洲洋持续消减和阿尔泰造山带向南增生造山的演化历史(Xiao et al., 2004, 2009),如图1。扎河坝—阿尔曼泰蛇绿岩带是早古生代古亚洲洋的分支——阿尔曼泰洋盆的遗迹(李锦铁,1991, 1995;何国琦等,2001),是准噶尔板块与西伯利亚板块间碰撞结合带(李荣社等,2012);卡拉麦里蛇绿岩形成于早—中泥盆世(肖序常和汤耀庆,1991),代表了泥盆纪分隔哈萨克斯坦—准噶

图1研究区构造单元图(据新疆地矿局修改^①)

I—西伯利亚板块; I-1—阿尔泰活动陆缘带; I-1-1—清河中间地块; I-1-2—震旦纪边缘海盆; I-1-3—乌恰沟-玛因鄂博晚古生代岛弧带; II—哈萨克斯坦-准噶尔板块; II-1—准噶尔北缘构造带; II-1-1—二台晚古生代复合岛弧带; II-1-2—乌伦古二叠纪上叠盆地; II-1-3—扎河坝—二台古生代沟弧带; II-1-4—库兰卡孜干晚古生代岛弧带; II-1-5—东准噶尔晚古生代陆缘盆地;

EMT—额尔齐斯-玛因鄂博缝合带

Fig.1 Tectonic division map of the study area (modified from Xinjiang Bureau of Geology and Mineral Resources)
I - Siberian plate; I - 1 - Altai active marginal zone; I - 1 - 1 - Qinghe intermediate massif; I - 1 - 2 - Sinia marginal basin; I - 1 - 3 - Wuqiaogou - Mayinebo late Paleozoic island arc belt; II - Kazakhstan - Junggar Plate; II - 1 - Northern margin of Junggar tectonic belt; II - 1 - 1 - Ertai late Paleozoic composite island arc belt; II - 1 - 2 - Wulungu Permian superimposed basin; II - 1 - 3 - Zhaheba - Ertai Paleozoic trench-arc belt; II - 1 - 4 - Kulankazigan late Paleozoic island arc belt; II - 1 - 5 - East Junggar late Paleozoic continental margin basin; EMT - Ertix - Mayinebo suture zone

尔板块与西伯利亚板块的古洋盆岩石圈残片(李锦轶, 1995)。扎河坝蛇绿岩是东准噶尔盆地—阿尔泰造山带内除卡拉麦里蛇绿岩带(产有清水铬铁矿)外第二处发现铬铁矿的蛇绿岩带,其构造演化与成矿意义重大。

区域上扎河坝—阿尔曼泰蛇绿岩带呈北西—南东走向位于东准噶尔中部,断续出露于北塔山北坡,阿尔曼泰山主脊及两侧和乌伦古河中下游,向

西延至唐巴勒—洪古勒楞一带,构成一条长达 600 km 的弧形蛇绿岩带(图1),是扎河坝—二台早古生代沟弧带的组成部分(张元元和郭召杰,2010)。

扎河坝蛇绿岩分布于扎河坝煤矿、萨热铁热克一带,长约 18 km,最大宽度 2 km,向北西、南东端逐渐尖灭,蕴都卡拉一带又有出露。受后期逆冲推覆构造影响(Li et al., 2014),呈透镜状残片叠置于中泥盆统火山岩、火山碎屑岩之上,与围岩均为断层接触。蛇绿岩岩石类型有蛇纹石化橄榄岩、层状辉长岩、玄武岩、紫红色放射虫硅质岩,也有代表大洋慢速扩张的斜长花岗岩和斜长岩(简平等,2003; Luo et al., 2017)及闪长岩、闪长玢岩侵入。

根据前人对蛇绿岩中发现早古生代牙形石及放射虫(李锦轶, 1991)、橄榄岩 Sm-Nd 等时线年龄(479 ± 27) Ma(刘伟和张湘炳, 1993)、层状辉长岩锆石 SHRIMP 年龄(489 ± 4) Ma(简平等, 2003)、斜长花岗岩锆石 U-Pb 年龄(494.6 ± 6.9) Ma(Zeng et al., 2015)、堆晶辉长岩锆石 U-Pb 年龄(485.8 ± 2.5) Ma(潘成泽等, 2016)、侵入于超镁铁质岩内的辉长岩体锆石 U-Pb 年龄(495.1 ± 3.5) Ma(Luo et al., 2017),结果显示该蛇绿岩带超基性岩形成早于 495 Ma,即超镁铁质岩的形成要早于晚寒武世。

3 超镁铁质岩与铬铁矿

3.1 超镁铁质岩

超镁铁质岩在扎河坝蛇绿岩带内广泛分布,但个体规模较小,受后期风化作用的影响,破碎较严重,地表多呈透镜体状残存。超镁铁质岩主要由强蛇纹石化方辉辉橄榄岩(比方辉橄榄岩中斜方辉石含量高)、二辉橄榄岩、方辉橄榄岩、少量纯橄榄岩和单辉橄榄岩组成,占超镁铁质岩体总面积的 85% 以上。从出露位置看,超铁镁质岩为蛇绿岩带最下部层位,上覆为镁铁质岩或硅质岩,局部与闪长岩、闪长玢岩和碳酸盐脉呈侵入接触(图 2)。岩石为块状、片状构造,墨绿色—黑色,纯橄榄岩、二辉橄榄岩手标本以缺少绢石区别于方辉橄榄岩。岩石蚀变以橄榄石的叶蛇纹石化、滑石化,斜方辉石绢石化及碳酸盐化为主。

3.2 铬铁矿

扎河坝蛇绿岩带内发现的“鸡窝状”铬铁矿(点)不同于典型的豆英状铬铁矿,可分两种矿石结

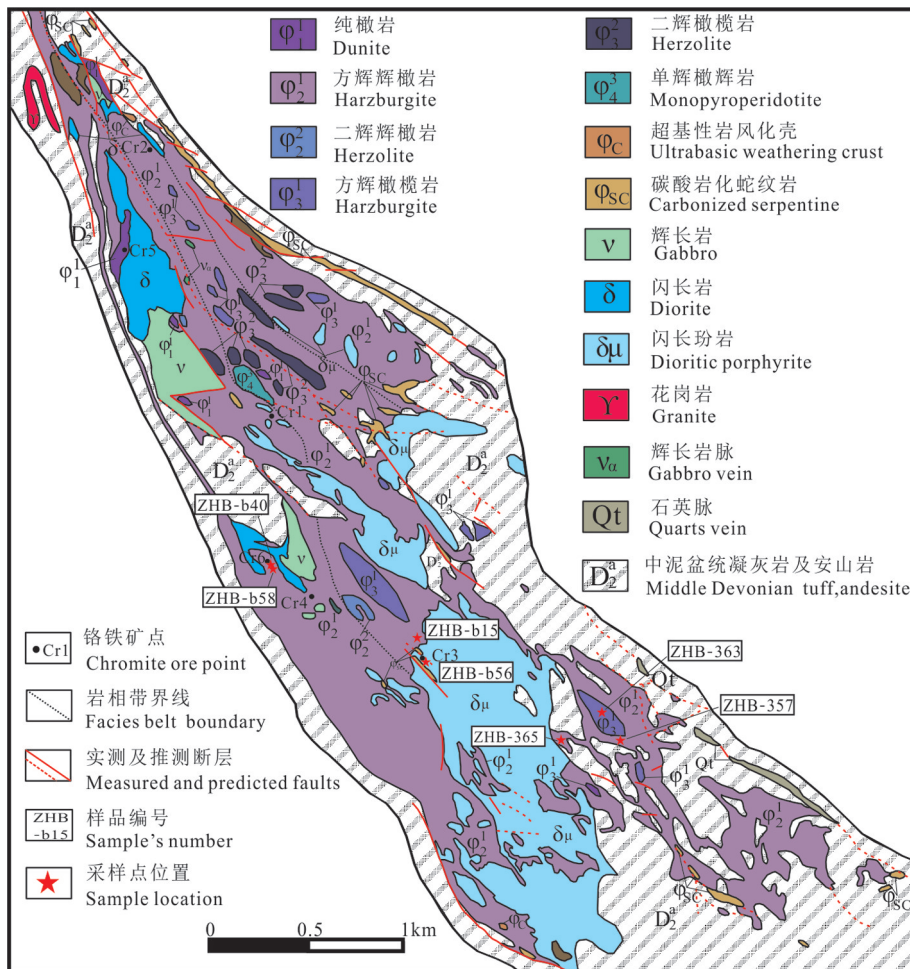


图2 扎河坝蛇绿岩地质图
Fig.2 Geological map of Zhaheba ophiolite

构:(1)碳酸盐胶结的角砾状(块状)铬铁矿;(2)透镜状、豆英状、不规则状铬铁矿。

角砾状(块状)铬铁矿:见于南带6号矿点碳酸盐化纯橄岩带内,有角砾状、碎裂状、裂纹状结构,被碳酸盐化纯橄岩胶结,显示铬铁矿形成早于碳酸盐化纯橄岩(图3a,b)。角砾状具有可拼合性,显示未经过长距离搬运,未见蚀变及溶蚀现象,说明碳酸盐胶结时铬铁矿已经固结;透镜状、豆英状、不规则状铬铁矿:见于中带3号矿点浅井及地表,“悬浮”于碳酸盐化纯橄岩中,铬铁矿与碳酸盐界限截然(图3c,d,e)。

4 岩相学特征

4.1 方辉辉橄岩

主要的造岩矿物为橄榄石(小于0.3 mm,含量

65%~70%),斜方辉石(主要为顽火辉石,0.5~5 mm,含量15%~20%),单斜辉石(主要为透辉石,0.2~2 mm,一般少于2%)以及6%~8%的铬尖晶石、磁铁矿等副矿物,斜方辉石含量变少可过渡为方辉橄岩。蚀变矿物有蛇纹石、绢石、少量绿泥石及碳酸盐。

方辉辉橄岩虽经历了强烈的蛇纹石化蚀变,但斜方辉石的绢石假晶或斜方辉石(主要是顽火辉石)绢石化残留晶在手表上可辨。

镜下观察发现,绢石化斜方辉石银灰色,呈他形,叶片状、不规则熔蚀状,解理纹清晰、平直,平行消光,矿物颗粒内发育膝折带(Kink-banding)、波状消光、扭折带,沿绢石化斜方辉石颗粒间及矿物解理有橄榄石定向出熔(图4a),蛇纹石化过程中析出的粒状磁铁矿,斜方辉石绢石化后发生波状消光,膝折带内有磁铁矿析出现象(图5a)。

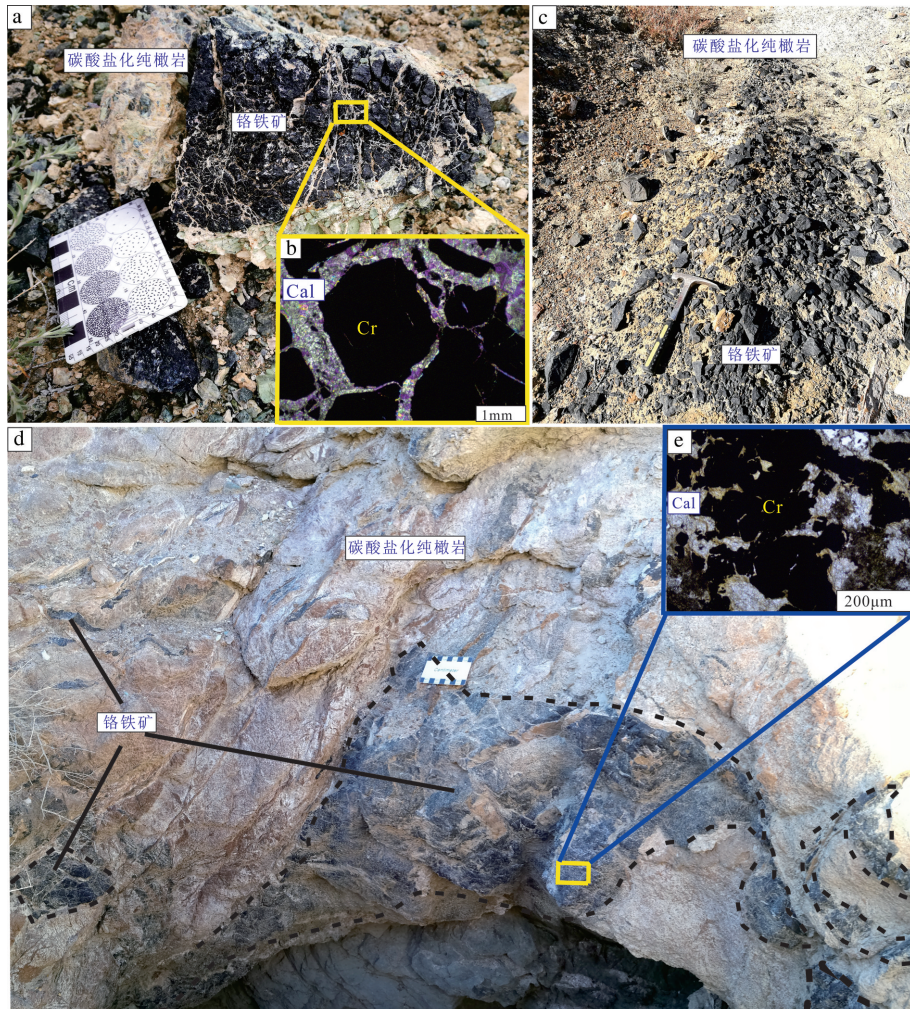


图3 扎河坝铬铁矿矿石照片

a—6号铬铁矿点角砾状、块状铬铁矿(ZHB-b40);b—铬尖晶石显微照片(ZHB-b40);c—3号铬铁矿点地表块状铬铁矿体;d—3号铬铁矿点浅井内块状铬铁矿;e—3号铬铁矿点块状铬铁矿显微照片(ZHB-b56)

Fig.3 Photoes and photomicrographs of Zhaheba chromite ore

a—No.6 chromite spot brecciated and massive chromite (ZHB-B40); b—Microphotograph of chrome spinel (ZHB-B40); c—Surface massive chromite orebody at No. 3 ore occurrence; d—Mmicrophotograph of massive chromite at the No. 3 ore occurrence (ZHB-B56)

4.2 二辉橄榄岩

主要的造岩矿物为橄榄石(小于0.3 mm, 60%~70%)、斜方辉石(主要为顽火辉石, 0.5~5 mm, 含量4%~10%)、单斜辉石(主为透辉石, 0.5~2 mm, 一般4%~8%), 铬尖晶石、磁铁矿等副矿物含量较少。橄榄石蛇纹石化强烈, 但仍有个别样品内核可见新鲜的橄榄石, 但外围已蚀变为蛇纹石。如图4b可见蛇纹石化二辉橄榄岩绢石化后斜方辉石残余, 中间为单斜辉石, 其边部及内部为新生橄榄石, 右上角蛇纹石内可见残留橄榄石。

与方辉辉橄榄岩内斜方辉石特征类似, 但明显可见斜方辉石保留着未完全绢石化后的残余特征, 常

可见有新生成的单斜辉石、橄榄石交代斜方辉石的现象, 这种单斜辉石、橄榄石不同于早期残余结构的透辉石和强蛇纹石化的橄榄石, 其矿物学特点是粒度较小, 呈锯齿状分布于斜方辉石(绢石)边部, 矿物几乎未发生蚀变。如图4c为蛇纹石化二辉橄榄岩, 照片右部为含橄榄石包体的斜方辉石及单斜辉石具熔融残余结构, 其左见众多新生橄榄石, 新生的单斜辉石叠加在斜方辉石上; 图4d为蛇纹石化二辉橄榄岩斜方辉石边部及楔形裂缝被后期形成的橄榄石和单斜辉石充填, 沿斜方辉石矿物解理有后期单斜辉石出溶, 呈锯齿状断续分布于斜方辉石边缘, 有的新生单斜辉石分布在具熔融残余结构单

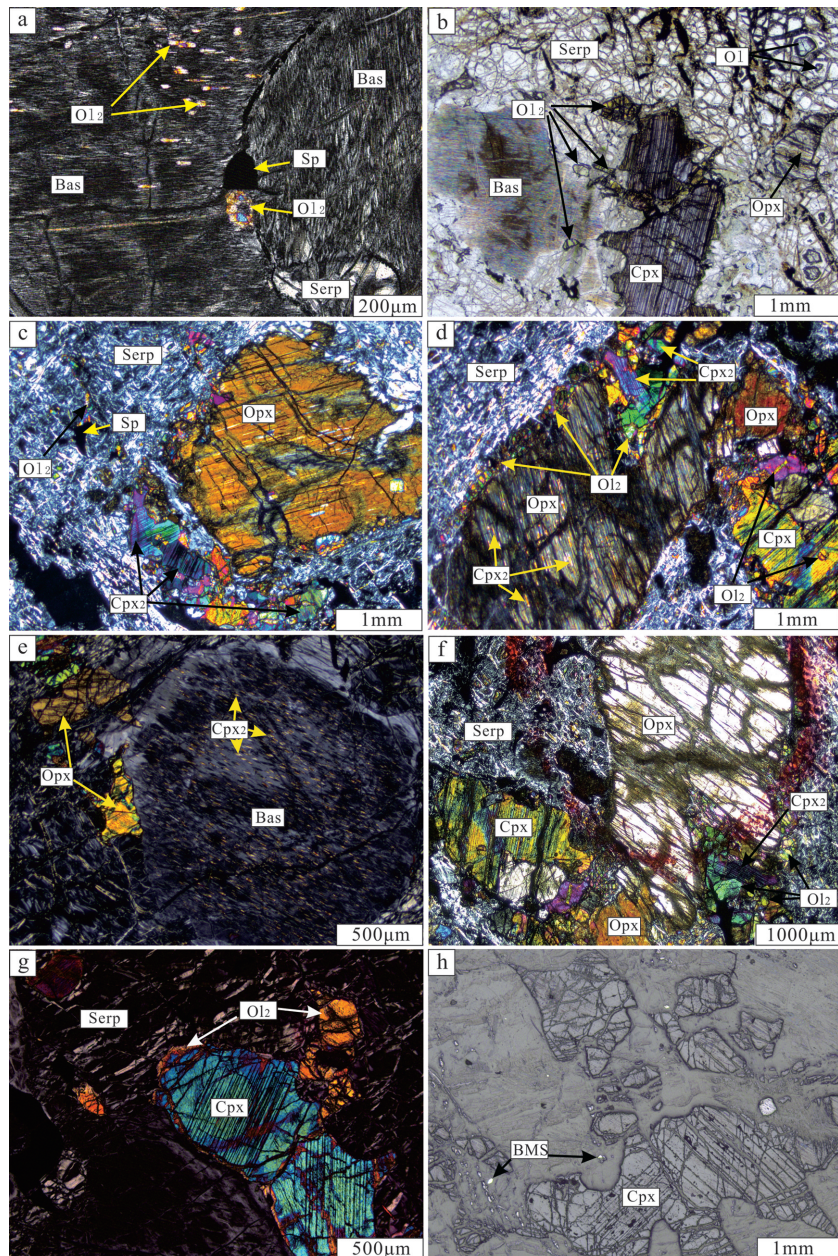


图4 扎河坝橄榄岩显微照片

a—ZHB-15样品方辉橄榄岩内铬尖晶石和新生橄榄石(正交偏光);b—Z19-26样品二辉橄榄岩斜方辉石残余、新生橄榄石和橄榄石残留晶(单偏光);c—Z19-25样品蛇纹石化二辉橄榄岩内熔融残余结构、新生橄榄石、新生的单斜辉石(正交偏光);d—Z19-25样品蛇纹石化二辉橄榄岩内新生的橄榄石、单斜辉石(正交偏光);e—D363样品二辉橄榄岩内熔融残余结构、新生单斜辉石(正交偏光);f—Z19-25样品蛇纹石化二辉橄榄岩内新生的橄榄石和单斜辉石(正交偏光);g—D363样品二辉橄榄岩内熔融残余结构、反应边结构(正交偏光);h—D363样品二辉橄榄岩熔融残余结构(反射光)。Opx—斜方辉石;Cpx—单斜辉石;Ol—橄榄石;Bas—绢石;Sp—尖晶石;Serp—蛇纹石;Ol2—新生橄榄石;Cpx2—新生的单斜辉石;BMS—贱金属硫化物

Fig.4 Microphotographs of Zhaheba peridotite

a—Chrome spinel and new olivine in harzburgite, cross-polar (ZHB-15); b—Orthopyroxene relicts, new olivine and olivine relicts in lherzolite, plane-polar (Z19-26); c—Structure of melted residual, new olivine, new clinopyroxene in serpentized lherzolite, cross-polar (Z19-25); d—New olivine, new clinopyroxene in serpentized lherzolite, cross-polar (Z19-25); e—Structure of melted residual, new clinopyroxene in lherzolite, cross-polar (D363); f—New olivine, new clinopyroxene in serpentized lherzolite, cross-polar (Z19-25); g—Structure of melted residual, reaction rim texture in lherzolite, cross-polar (D363); h—Structure of melted residual in lherzolite, cross-polar, reflected light (D363). Opx—Orthopyroxene; Cpx—Clinopyroxene; Ol—Olivine; Bas—Bastite; Sp—Spinel; Serp—Serpentine; Ol2—New olivine; Cpx2—New clinopyroxene; BMS—Base metal sulfides

斜辉石的边缘);图4f为蛇纹石化二辉橄榄岩,斜方辉石右边部及下部为新生的单斜辉石和橄榄石;单斜辉石边部及解理内可见不规则状铬铁矿出溶,而且可见脉状蛇纹石及绢石化斜方辉石叠加在残留的单斜辉石上,显示蛇纹石化、绢石化发生在单斜辉石熔融残余之后,这种单斜辉石呈他形,解理及裂隙发育,呈不规则熔蚀状,矿物边缘变成复杂的港湾状、锯齿状、蚕食状,形成熔融残余结构,蛇纹石化橄榄石颗粒间含贱金属硫化物及磁铁矿析出(图4e、g、h)。

4.3 纯橄岩

纯橄岩内橄榄石几乎全部蛇纹石化、滑石化,仅局部保留着橄榄石晶形,呈网状、信封状及叶片状结构,具有波状消光,纤蛇纹石组成网架,中间为叶蛇纹石,颗粒边部有磁铁矿析出。蛇纹石矿物主要为叶蛇纹石,也有少量纤蛇纹石和利蛇纹石,构成了特征性的“网眼”(mesh)结构。

磁铁矿呈“龟背纹状”、颗粒填隙状、脉状围绕蛇纹石颗粒和绢石化斜方辉石解理、膝折处,反映蛇纹石化过程中磁铁矿由橄榄石和斜方辉石释放出来。晚期脉状碳酸盐沿着蚀变的斜方辉石解理并穿蛇纹石发育。

单斜辉石:含量小于4%,主要是透辉石,呈淡绿色、灰黑、灰白色等,一般为似斑状或糖粒状,大小不均匀,粒径0.2~1 mm。原生的单斜辉石(主要是透辉石)多呈熔融残余结构,新生的单斜辉石呈单晶或在斜方辉石边缘呈细粒连晶,解理和裂纹一般较绢石和斜方辉石粗,且不平直,常具有弯曲和斜消光现象。

斜长石:少量,呈灰绿、灰白色,他形粒状,油脂光泽,粒度小于1 mm,分布于蛇纹石、辉石颗粒之间,多蚀变为绿泥石、黏土矿物。

铬尖晶石:多见于纯橄岩、方辉橄榄岩内,以尖晶石副矿物形式存在,呈他形分布于蛇纹石化橄榄石或辉石颗粒间,0.1~0.5 mm,透明度差,仅在强光下可见微弱褐色或棕褐色,含量0.5%~1%,多呈蠕虫状、港湾状、熔蚀状,个别样品见自形一半自形(图5a、b、c),BSE图像显示矿物边部及裂隙处常见反射率更强的蚀变带或薄边(图5e、f、h),这种现象被认为是沿尖晶石边部、裂隙有后期磁铁矿蚀变、交代变为铁铬铁矿(Ferrichromite)(Evans and

Frost, 1975; Barnes, 2000)。存在于块状、透镜状、不规则状铬铁矿内的铬尖晶石,矿物颗粒粗大,一般0.5~2 cm,显微镜下显示强反射性,碳酸盐胶结的碎裂结构、角砾状结构,局部具有可拼合性(图5g、d)。

5 样品和分析方法

本次样品主要采集于扎河坝蛇绿岩地表的新鲜橄榄岩及铬铁矿矿石。经过室内的样品初步筛选,选出具有代表性样品磨制探针片,经徕卡偏光显微镜进行观察鉴定、拍照以及探针点初步选取等工作。本次电子探针分析样品共8件,其中3件为块状铬铁矿矿石、5件为含铬尖晶石副矿物的橄榄岩。电子探针成分分析前首先使用真空镀膜仪对所精选样品进行镀碳,随后对已镀好碳膜的薄片进行探针分析,该工作是在天津地质调查中心实验室完成,实验仪器为:日本电子公司EPMA1600,测试条件:探针束流20 nA,加速电压15.0 kV,电子束斑直径1 μm,分析元素包括Al、Cr、Ca、Mg、Si等9种元素。分析过程不损坏样品,全成分分析误差<2%。同时可满足对样品的SE、BSE物象分析和波谱、能谱成分分析的要求。

6 分析结果

6.1 单斜辉石

单斜辉石是橄榄岩的主要矿物,二辉橄榄岩样品D363电子探针数据分析表明,具有熔融残余结构的单斜辉石属于透辉石,氧化物含量:Cr₂O₃ 0.79%~1.30%,平均1.11%,Al₂O₃ 3.58%~5.43%,平均4.77%,MgO 15.04%~26.23%,平均16.99%,CaO 15.12%~23.05%,平均21.84%,SiO₂ 45.98%~51.57%,平均50.00%。其Mg[#]为0.90~0.95,Cr[#]为0.12~0.17,平均0.14。

单斜辉石的Cr₂O₃与Al₂O₃、SiO₂与MgO之间为正相关关系,Cr₂O₃和Al₂O₃均与MgO呈反相关关系(图6),反映随着部分熔融程度的增高,单斜辉石释放出其晶格间Cr、Al,成为铬铁矿的物质来源之一,其化学成分总体向更加富Si、富Mg的方向进行演化。Al₂O₃与SiO₂、MgO与FeO相关关系不明显。

6.2 块状铬铁矿铬尖晶石

铬尖晶石各元素含量变化较小:Cr₂O₃ 52.62%~57.22%,平均55.45%,Al₂O₃ 7.29%~14.45%,平均

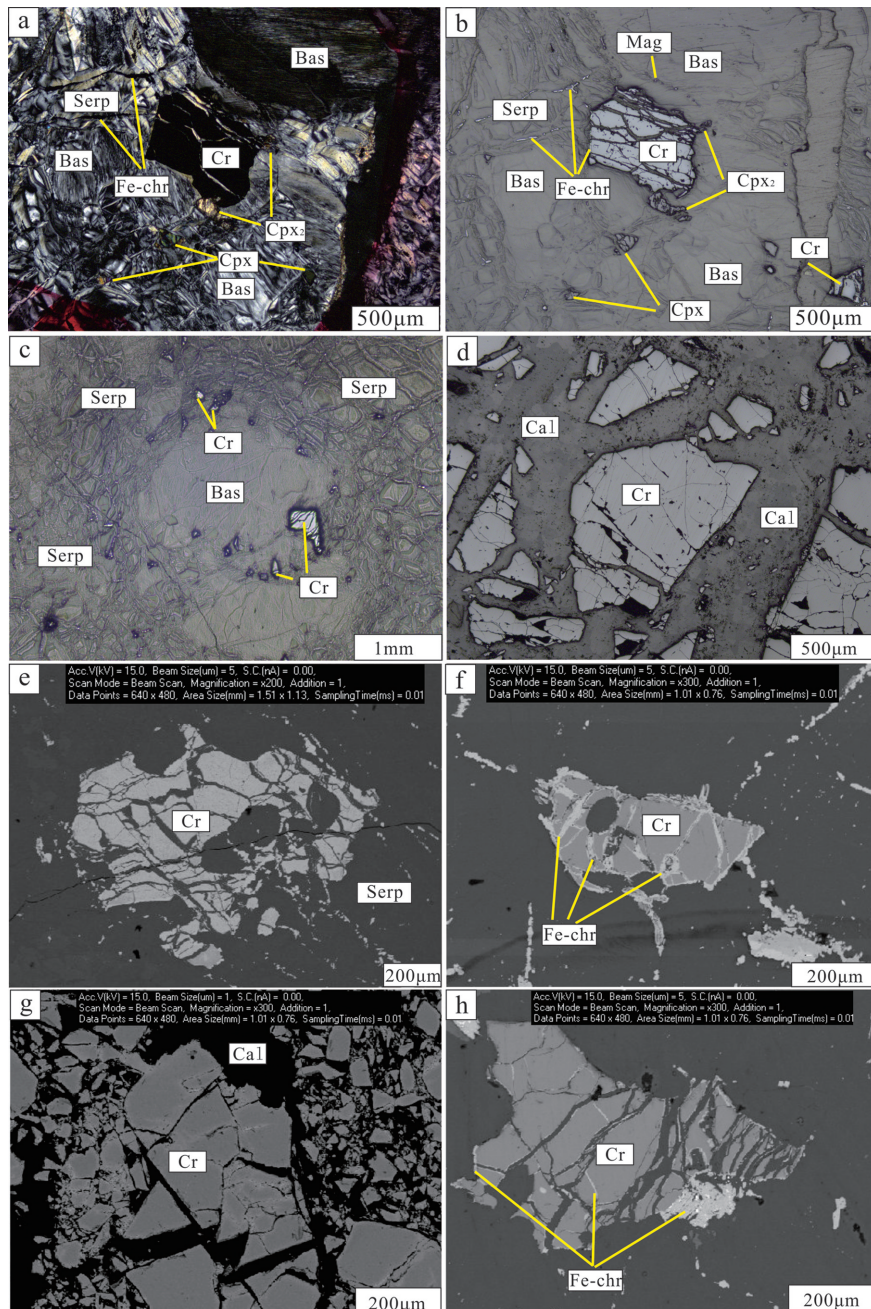


图5 橄榄岩尖晶石副矿物、块状铬铁矿镜下照片及背散射图像

a(正交偏光)、b(反射光)—D15样品方辉橄榄岩内新生单斜辉石及铬尖晶石边部发生磁铁矿化; c—ZHB-b15样品方辉橄榄岩内半自形铬尖晶石及不规则状铬尖晶石残留; d—3号铬铁矿点ZHB-b40样品角砾状铬铁矿反射光照片; e—D357样品方辉橄榄岩内铬尖晶石熔蚀结构背散射(BSE)照片; f、h—D15样品方辉橄榄岩背散射(BSE)照片, 尖晶石副矿物熔蚀结构及其边部、裂隙处铁铬铁矿(Fe-chr); g—3号铬铁矿点碎裂状、块状铬铁矿尖晶石背散射(BSE)照片; Cpx—单斜辉石; Bas—绢石; Cr—铬铁矿; Serp—蛇纹石; Cal—碳酸盐; Cpx₂—新生单斜辉石; Fe-chr—铁铬铁矿; Mag—磁铁矿

Fig.5 Microphotograph of spinel in peridotite and back scattered electron images (BSE) of spinels in massive chromite
 a (cross-polar), b (reflected light) — New clinopyroxene, magnetization occurs at the edge of chrome spinel in harzburgite (D15); c — Subhedral chrome spinel, irregular chrome spinel relicts in harzburgite, reflected light (ZHB-b15); d — Photomicrographs of brecciaous chromitite in No. 3 chromite point, reflected light (ZHB-b40); e — BSE images of chrome spinel with melting corrosion structure in harzburgite (D357); f, h — BSE images of chrome spinel with melting corrosion structure, altered to ferritchromite (Fe-chr) along it's cracks and edges in harzburgite (D15); g — BSE images of chrome spinel of fractured, massive chromites in No.3 chromite point; Cpx — Clinopyroxene; Bas — Bastite; Cr — Chromite; Serp — Serpentine; Cal — Carbonate; Cpx₂ — New clinopyroxene; Fe-chr — Ferritchromite; Mag — Magnetite

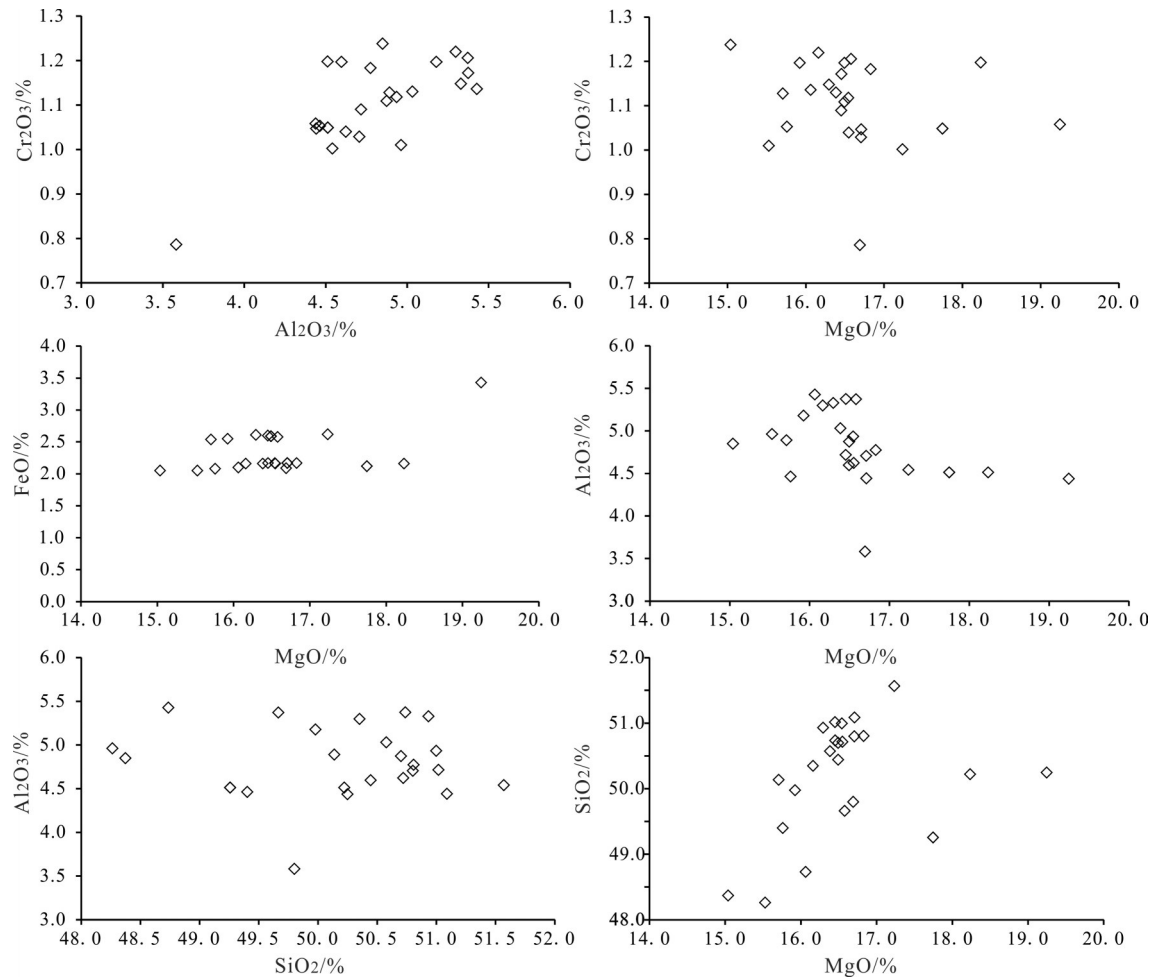


图6 单斜辉石主要氧化物关系图解
Fig.6 Diagram showing the relationship among major oxides of the clinopyroxene

10.88%, MgO 10.83%~13.54%, 平均 11.98 %, Mg[#] 0.60, Cr[#](0.72~0.84) 平均 0.77, Cr/Mg 为 2.47。在 Cr₂O₃-Al₂O₃ 图解中样品落入豆英状铬铁矿和罗布莎高 Cr 铬铁矿范围内, 而远离层状铬铁矿和萨尔托海高 Al 铬铁矿、土耳其高 Al 铬铁矿范围(图 7); 在 Mg[#]-Cr[#] 图解中, 样品位于高 Cr 区域, 落入玻安质熔浆和 SSZ 型橄榄岩范围内, 大部分落入罗布莎高 Cr 铬铁矿范围内, 但比其具有更高的 Cr[#] 值(图 8)。Cr/Fe-Cr[#] 图解中大部分落在深部地幔铬铁岩区, 少部分落在 MOHO 面下浅部地幔铬铁岩区(图 9)。

6.3 橄榄岩内副矿物尖晶石

铬尖晶石电子探针分析结果见表 1, 铬尖晶石内部具有比块状铬铁矿更低的 Cr₂O₃ (38.96%~42.15 %, 平均 40.35%)、Cr[#](0.50~0.56, 平均 0.53) 和更高的 Al₂O₃(22.59%~26.04 %, 平均 24.10 %), MgO

(平均 13.23%) 和 Mg[#](0.62) 比块状铬铁矿略高, 而 FeO 含量与块状铬铁矿基本相当。Cr/Mg 较低, 为 1.62。在 Cr₂O₃-Al₂O₃ 图解中样品落入层状铬铁矿范围内, 而远离豆英状铬铁矿和高 Al 铬铁矿范围(图 7)。在 Mg[#]-Cr[#] 图解中, 虽然样品位于高 Al 区域及豆英状铬铁矿和罗布莎高 Cr 铬铁矿范围内, 但明显远离玻安质熔浆范围(图 8)。副矿物铬尖晶石高 Cr/Fe 值一般代表含矿蛇绿岩的地球化学特征(刘婷等, 2019), 在 Cr[#]-Cr/Fe 图解中落在堆晶纯橄岩及萨尔托海高 Al 铬铁矿范围内。可见, 副矿物尖晶石具高 Al、低 Ti 特征, 落入深海型 abyssal 橄榄岩区, 显示 MORB 型橄榄岩亲和性(图 9)。

铬尖晶石边部及裂隙处成分变化较大, 与铬尖晶石内部元素含量也具有明显差异: FeO(平均 25.88%)、Fe₂O₃(平均 40.69%)、MnO(平均 2.85%)、

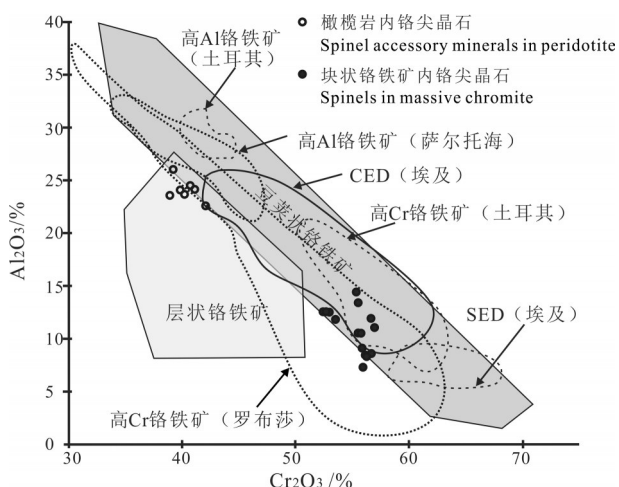


图7 橄榄岩内尖晶石副矿物、块状铬铁矿尖晶石
 Al_2O_3 – Cr_2O_3 含量(%)图解

(层状铬铁矿、豆英状铬铁矿数据范围参考 Bonavia et al., 1993; 土耳其高 Cr、高 Al 铬铁矿数据范围参考 Uysal et al., 2009; 埃及 CED 铬铁矿数据范围参考 Ahmed et al., 2001; 萨尔托海数据范围参考 Zhou et al., 2014; 罗布莎数据范围参考 周二斌等, 2011, 下同)

Fig. 7 Al_2O_3 versus Cr_2O_3 (%) diagram of spinels in peridotite and massive chromite

Compositional fields of stratiform and podiform chromitites are from Bonavia et al., 1993; High-Cr and high-Al compositional fields of SW Turkey (Uysal et al., 2009); Central and southern Eastern Desert (CED, SED) of Egypt (Ahmed et al., 2001); Compositional fields of Sartohay (Zhou et al., 2014); Compositional fields of Luobusha (Zhou, 2011)

NiO (平均 0.41 %)等含量明显升高, Al_2O_3 (0.25%~5.73 %, 平均 1.53 %)、 Cr_2O_3 (9.49%~23.50 %, 平均 17.97 %)、 MgO (平均 4.07 %)和 $\text{Mg}^{\#}$ (0.22)含量明显降低, 由于 Al 、 Mg 含量降低、 Fe^{3+} 含量升高, $\text{Cr}^{\#}$ 、 Cr/Mg 及 Fe^{3+} 明显升高, 分别为 0.88、5.95 和 0.62。

7 讨 论

7.1 部分熔融程度与地幔橄榄岩类型、矿物类型、成分的变化及铬铁矿形成

地幔熔融程度是控制地幔岩石类型、尖晶石成分及铬铁矿 Cr_2O_3 、 Al_2O_3 等含量变化的因素 (Dick and Bullen, 1984): 即富 Cr、低 Al 的铬铁矿是高程度部分熔融的结果, 富 Al–低 Cr 型铬铁矿与相对低程度部分熔融形成的拉斑质熔浆有关 (Zhou and Robinson, 1994; Uysal et al., 2009; Ahmed and Abdelmonem, 2015)。

扎河坝块状铬铁矿内造矿铬尖晶石具高 Cr、低 Al 的特征, 橄榄岩内副矿物铬尖晶石具有高 Al 的特

点, 显然二者是不同熔融事件的产物 (图 7)。在 $\text{Cr}^{\#}$ – $\text{Mg}^{\#}$ 图解中 (图 8), 橄榄岩内副矿物尖晶石落入 SSZ 橄榄岩与 Abyssal 橄榄岩交汇区, 而块状铬铁矿尖晶石落入 SSZ 橄榄岩和玻安质熔浆区, 说明副矿物尖晶石相比于块状铬铁矿尖晶石的橄榄岩母熔体的部分熔融程度更低。副矿物铬尖晶石与块状铬铁矿其尖晶石的 Al_2O_3 与 Cr_2O_3 均呈负相关关系, 即随着部分熔融程度的增大, 铬尖晶石残留相中 Al_2O_3 更加亏损, 但与扎河坝橄榄岩内铬尖晶石副矿物相比, Cr_2O_3 含量较高, 而 Al_2O_3 明显较低 (图 7)。同时也发现如单斜辉石 (透辉石) 含量更高的二辉橄榄岩 (如样品 ZHB363) 其铬尖晶石的 Cr_2O_3 含量及 $\text{Cr}^{\#}$ 明显低于方辉橄榄岩, 而 SiO_2 、 Al_2O_3 含量明显高于方辉橄榄岩, 即随着熔融程度的提高, 铬尖晶石 Cr 含量升高, 而 Si、Al 的含量降低。

虽然从二辉橄榄岩到方辉橄榄岩的演化过程中, 元素含量发生明显变化, 扎河坝方辉橄榄岩内斜方辉石 Cr_2O_3 含量为 0.79%~1.3%、铬尖晶石副矿物 Cr_2O_3 含量为 38.96%~42.15%, 大于鲍佩声 (2009) 统计的世界范围内幔源包体单斜辉石、副矿物铬尖晶石 Cr_2O_3 含量 (分别为 0.38%、0.76%), 说明部分熔融过程中辉石、副矿物铬尖晶石为铬的富集及块状铬铁矿的形成起重要作用。但要形成品位大于 20% 的铬矿石, 要求地幔岩部分熔融程度应该在 85% 以上 (熊发辉等, 2013), 然而大部分 SSZ 背景的方辉橄榄岩和纯橄岩其部分熔融程度也只有 21%~22%, 而 MORB 背景的方辉橄榄岩和纯橄岩其部分熔融程度也只有 17%~18% (Ahmed and Abdelmonem, 2015), 因此简单的部分熔融和低程度部分熔融时方辉橄榄岩内尖晶石副矿物可能无法为铬铁矿的形成提供足够的铬源 (Zhou et al., 1996)。

7.2 铬来源及矿床成因

近年来关于铬来源及矿床成因问题也形成两种主流观点, 即: 地幔橄榄岩矿物相转变, 含铬矿物释放一辉石不一致熔融、铬尖晶石副矿物熔化和熔–岩反应。前者认为铬铁矿中铬主要来自于地幔橄榄岩中含铬矿物释放, 即铬透辉石、顽火辉石的不一致熔融和对副矿物铬尖晶石的改造 (王希斌和鲍佩声, 1987; 郝梓国, 1991; 鲍佩声, 2009)。然而, 后者认为熔–岩反应主要是玻安岩熔体与方辉橄榄岩反应 (Zhou and Robinson, 1994; Zhou et al., 1998;

表1 块状铬铁矿内铬尖晶石及橄榄岩铬尖晶石副矿物、单斜辉石电子探针数据(%)及参数统计

Table 1 Electron microprobe analyses of spinels in massive chromite and peridotite and clinopyroxene

序号	点号	Cr ₂ O ₃	TiO ₂	Al ₂ O ₃	Fe ₂ O ₃	FeO	MgO	MnO	NiO	CaO	SiO ₂	Total	Mg [#]	Cr [#]	Fe ²⁺ /	Fe ^{3+)/(Cr+)}	Al/(Cr+)	Mg/	Cr/Fe
															(Fe ²⁺ +Mg)	Al+Fe ³⁺)	Al+Fe ³⁺)	(Mg+Fe ²⁺)	
1	ZHB-b40-1	55.74	0.13	10.55	4.81	14.77	11.70	0.28	0.14	0.01	0.00	97.71	59.00	78.00	0.41	0.06	0.21	0.59	2.75
2	ZHB-b40-2	57.22	0.14	11.07	4.08	15.05	11.78	0.32	0.14	0.01	0.02	99.56	58.59	77.62	0.41	0.05	0.21	0.59	2.87
3	ZHB-b40-3	56.01	0.13	10.52	4.39	13.65	12.20	0.30	0.16	0.01	0.00	97.02	61.62	78.13	0.38	0.05	0.21	0.62	2.99
4	ZHB-b40-4	56.89	0.11	11.94	3.29	15.53	12.06	0.29	0.05	0.00	0.02	99.74	58.42	76.17	0.42	0.04	0.23	0.58	2.93
5	ZHB-b40-5	55.74	0.11	13.43	3.76	16.15	11.69	0.33	0.10	0.00	0.00	101.10	56.57	73.58	0.43	0.04	0.25	0.57	2.68
6	ZHB-b56	55.58	0.44	14.45	2.53	13.67	13.54	0.29	0.12	0.01	0.01	100.55	64.00	72.08	0.36	0.03	0.27	0.64	3.26
7	ZHB-b56-2	52.62	0.43	12.57	3.99	13.28	12.70	0.29	0.20	0.01	0.03	95.55	63.37	73.74	0.37	0.05	0.25	0.63	2.98
8	ZHB-b56-3	53.18	0.43	12.52	3.60	13.31	12.77	0.30	0.15	0.00	0.00	95.77	63.37	74.02	0.37	0.04	0.25	0.63	3.06
9	ZHB-b56-5	53.74	0.44	11.83	4.00	13.30	12.69	0.32	0.10	0.00	0.03	96.11	63.37	75.30	0.37	0.05	0.23	0.63	3.00
10	ZHB-b56-6	52.89	0.45	12.57	4.01	13.36	12.80	0.32	0.17	0.00	0.03	96.12	63.37	73.85	0.37	0.05	0.25	0.63	2.96
11	ZHB-b58-1	56.92	0.16	8.61	4.71	15.18	11.23	0.35	0.17	0.00	0.06	96.75	57.43	81.61	0.43	0.06	0.17	0.57	2.79
12	ZHB-b58-2	56.39	0.15	8.45	4.30	15.84	11.00	0.32	0.16	0.00	0.44	96.61	55.45	81.75	0.45	0.06	0.17	0.55	2.71
13	ZHB-b58-3	56.19	0.12	7.29	6.13	13.80	11.38	0.32	0.12	0.01	0.02	94.71	60.00	83.80	0.40	0.08	0.15	0.6	2.76
14	ZHB-b58-4	56.10	0.15	9.12	5.10	14.84	11.30	0.29	0.12	0.01	0.02	96.52	58.00	80.49	0.42	0.06	0.18	0.58	2.73
15	ZHB-b58-5	56.51	0.14	8.31	4.65	15.33	10.83	0.32	0.11	0.00	0.00	95.79	56.00	82.02	0.44	0.06	0.17	0.56	2.73
16	ZHB-b15-1	40.26	0.18	23.70	5.09	13.75	13.62	0.24	0.13	0.02	0.04	96.47	64.36	53.26	0.36	0.06	0.44	0.64	2.08
17	ZHB-b15-5-5	38.96	0.17	23.58	5.01	15.40	12.41	0.26	0.04	0.04	0.06	95.52	59.41	52.57	0.41	0.06	0.45	0.59	1.85
18	ZHB-b15-5-2	41.18	0.20	24.16	5.20	14.44	13.65	0.25	0.10	0.01	0.03	98.76	63.00	53.35	0.37	0.06	0.44	0.63	2.03
19	ZHB-b15-5-7	40.78	0.27	24.52	5.21	14.45	13.54	0.27	0.13	0.00	0.00	98.81	63.00	52.73	0.37	0.06	0.44	0.63	2.00
20	ZHB-b15-5-7-1	39.88	0.15	24.10	6.02	14.31	13.52	0.26	0.14	0.01	0.02	97.82	63.00	52.61	0.37	0.07	0.44	0.63	1.91
21	ZHB-b15-5-8	42.15	0.25	22.59	5.12	16.89	11.92	0.30	0.14	0.00	0.02	98.98	56.00	55.59	0.44	0.06	0.42	0.56	1.85
22	ZHB-b15-5-9	39.27	0.18	26.04	4.35	14.09	13.92	0.23	0.18	0.03	0.05	98.06	64.00	50.29	0.36	0.05	0.47	0.64	2.05
23	ZHB-b15-4-1	9.49	0.04	5.73	53.43	30.01	2.83	0.19	0.16	0.09	1.25	98.00	16.98	52.63	0.83	0.70	0.14	0.17	0.11
24	ZHB-363-1	1.22	0.23	5.30	0.00	2.16	16.16	0.09	0.05	22.86	50.35	98.99	92.19	13.38	0.08	0.00	0.87	0.92	0.51
25	ZHB-363-2-1	1.17	0.22	5.37	0.00	2.17	16.45	0.07	0.05	22.72	50.74	99.55	92.31	12.76	0.08	0.00	0.87	0.92	0.48
26	ZHB-363-2-2	1.05	0.23	4.44	0.00	2.17	16.71	0.05	0.08	23.05	51.09	99.26	92.42	13.65	0.08	0.00	0.86	0.92	0.46
27	ZHB-363-2-3	1.00	0.23	4.54	0.00	2.62	17.24	0.07	0.08	21.91	51.57	99.73	91.30	12.89	0.09	0.00	0.87	0.91	0.35
28	ZHB-363-2-5	1.18	0.21	4.77	0.00	2.17	16.83	0.13	0.06	22.69	50.81	99.53	92.42	14.25	0.08	0.00	0.86	0.92	0.47
29	ZHB-363-2-6	1.09	0.25	4.72	0.00	2.60	16.45	0.11	0.00	22.74	51.02	98.83	90.91	13.42	0.09	0.00	0.87	0.91	0.42
30	ZHB-363-3	1.21	0.24	5.37	0.00	2.58	16.58	0.06	0.05	22.55	49.66	98.65	91.04	13.09	0.09	0.00	0.87	0.91	0.48
31	ZHB-363-3-1	1.04	0.27	4.62	0.00	2.16	16.55	0.10	0.04	22.90	50.72	99.00	92.42	13.11	0.08	0.00	0.87	0.92	0.43
32	ZHB-363-3-3	1.20	0.20	5.18	0.00	2.55	15.92	0.09	0.10	22.11	49.98	97.71	90.77	13.42	0.09	0.00	0.87	0.91	0.47
33	ZHB-363-4	1.14	0.19	5.43	0.00	2.10	16.06	0.07	0.03	21.92	48.74	96.36	92.42	12.31	0.08	0.00	0.88	0.92	0.47
34	ZHB-363-4-1	0.79	0.16	3.58	0.00	2.09	16.69	0.08	0.05	21.88	49.80	95.64	92.65	12.83	0.07	0.00	0.87	0.93	0.34
35	ZHB-363-4-2	1.01	0.16	4.96	0.00	2.05	15.53	0.03	0.00	21.42	48.26	94.14	92.31	12.01	0.08	0.00	0.88	0.92	0.44
36	ZHB-363-5	1.15	0.25	5.33	0.00	2.61	16.30	0.11	0.07	22.60	50.93	99.84	90.77	12.63	0.09	0.00	0.87	0.91	0.43
37	ZHB-363-5-2	1.30	0.14	4.20	0.00	2.18	26.23	0.08	0.14	15.12	45.98	95.74	95.19	17.15	0.05	0.00	0.83	0.95	0.52
38	ZHB-363-5-3	1.12	0.22	4.94	0.00	2.17	16.54	0.09	0.07	22.89	51.00	99.65	92.31	13.19	0.08	0.00	0.87	0.92	0.46
39	ZHB-363-5-5	1.24	0.22	4.85	0.00	2.05	15.04	0.07	0.06	21.92	48.37	94.49	92.06	14.62	0.08	0.00	0.85	0.92	0.52
40	ZHB-363-7	1.20	0.18	4.60	0.00	2.59	16.49	0.08	0.00	22.97	50.44	98.80	91.04	14.87	0.09	0.00	0.85	0.91	0.47
41	ZHB-363-7-2	1.11	0.24	4.87	0.00	2.59	16.49	0.09	0.05	22.69	50.70	99.13	90.91	13.24	0.09	0.00	0.87	0.91	0.44
42	ZHB-363-8	1.13	0.24	5.03	0.00	2.16	16.39	0.08	0.05	22.71	50.58	99.02	92.31	13.09	0.08	0.00	0.87	0.92	0.46
43	ZHB-363-8-1	1.03	0.20	4.71	0.00	2.17	16.71	0.07	0.00	22.90	50.80	99.25	92.42	12.79	0.08	0.00	0.87	0.92	0.42
44	ZHB-363-8-2	1.05	0.20	4.46	0.00	2.08	15.76	0.07	0.07	21.78	49.40	95.53	92.31	13.66	0.08	0.00	0.86	0.92	0.45
45	ZHB-363-10	1.13	0.27	4.89	0.00	2.54	15.71	0.12	0.04	21.96	50.14	97.15	90.77	13.40	0.09	0.00	0.87	0.91	0.45
46	ZHB-363-10-1	1.06	0.20	4.44	0.00	3.43	19.25	0.10	0.08	18.17	50.25	97.18	89.87	13.79	0.10	0.00	0.86	0.9	0.31
47	ZHB-363-10-2	1.20	0.19	4.51	0.00	2.16	18.23	0.09	0.03	21.38	50.22	98.26	93.06	15.12	0.07	0.00	0.85	0.93	0.55
48	ZHB-363-10-3	1.05	0.20	4.51	0.00	2.12	17.75	0.08	0.04	20.97	49.26	96.40	93.06	13.49	0.07	0.00	0.87	0.93	0.48
49	ZHB-363-11	1.05	0.20	4.51	0.00	2.12	17.75	0.08	0.04	20.97	49.26	96.40	93.06	13.49	0.07	0.00	0.87	0.93	0.48
50	ZHB-363-5-1	15.83	0.19	1.98	33.10	22.84	8.31	4.26	0.37	0.26	7.61	91.30	42.02	84.28	0.58	0.60	0.06	0.42	0.29
51	ZHB-363-3-2	15.86	0.12	3.11	28.22	21.71	9.91	4.45	0.28	0.11	9.12	90.32	47.15	77.38	0.53	0.54	0.10	0.47	0.32
52	ZHB-363-10-4	15.44	0.11	2.03	33.23	22.34	8.24	4.35	0.40	0.17									

Melcher et al., 1999; Kamenetsky et al., 2001; Uysal et al., 2005, 2009; González et al., 2011; Zaccarini et al., 2011)。

Cr是相容元素,如果熔融残余形成大规模铬铁矿的观点成立,那么铬铁矿应该最富Cr、Mg等相容元素,而最亏损Al、Ti、Fe等不相容元素,而本文橄榄岩铬尖晶石副矿物具有低于块状铬铁矿尖晶石的Mg[#],说明铬铁矿的形成不能单纯地用部分熔融和含铬矿物熔融来解释。类似的,新疆萨尔托海高Al型铬铁矿也不能代表最高度熔融的上地幔残余产物(周美付和白文吉,1994),西藏罗布莎高铬型铬铁矿床从纯橄榄岩外壳中铬尖晶石分区至造矿铬尖晶石分区反映了Cr[#]基本不变,而Mg[#]增加的过程,铬铁矿的围岩中副矿物铬尖晶石与铬铁矿中造铬尖晶石的形成过程呈负相关性,无法用简单的耐火残余部分熔融的观点来解释(熊发挥等,2013,2014)。因此,含铬矿物熔融、释放是铬来源的一种方式,单斜辉石熔融残余结构只是熔融程度逐渐增高,向更富镁方向演化的结构标志,对富Cr型铬铁矿的形成贡献有限。

此外,“熔融残余”结构模式无法解释早期发生熔蚀的辉石边部新生的辉石、橄榄石成因(Seyler et al., 2007)。橄榄岩中新生单斜辉石是晚期熔体与寄主橄榄岩交代(熔-岩反应)作用叠加的产物(Zhou et al., 2001; 黄启帅等, 2012),或是源自熔体重结晶(Seyler et al., 2001; Eric et al., 2002; Daniele et al., 2006),进而产生玄武质熔体部分熔融后的再富集(Elthon, 1992)。新生的单斜辉石以小颗粒、蚀变微弱、沿早期橄榄岩中的单斜辉石边部发育而区别,是熔-岩反应的结构和矿物学证据(Zhou et al., 2001; Seyler et al., 2007)。因此,也有人认为二辉橄榄岩和方辉橄榄岩中单斜辉石、铬铁矿内有斜方辉石残留是熔-岩反应不完全或低熔/岩比的结果(Su et al., 2019)。熔-岩反应的核心观点认为熔体在上升运移过程中与周围的地幔橄榄岩发生反应时地幔橄榄岩内斜方辉石熔解转化为橄榄石,释放铬的同时增加岩浆中SiO₂含量,SiO₂的增加降低了Cr的溶解度,进而引发铬铁矿沉淀(Zhou and Robinson, 1994; Arai and Yurimoto, 1994; Zhou et al., 1996, 1997, 1998)。然而,熔岩反应过程中流体、挥发分的因素不能被忽视(田亚洲和杨经绥, 2016; 苏本勋

等,2018; 罗照华等,2019),熔-岩反应过程中由于新生单斜辉石的沉淀也几乎不可能形成完全由橄榄石组成的纯橄榄岩,且与铬铁矿成生关系密切的包壳纯橄榄岩(Arai and Yurimoto, 1994; Arai, 1997; Zhou et al., 1996)形成过程中也有大量深部流体、挥发分参与的证据,因此对缺少流体、挥发分参与的熔-岩反应可以形成大规模包壳纯橄榄岩和铬铁矿的说法提出质疑,并提出“熔体-流体流”成因模型(罗照华等,2019)。

在矿物学、结构学方面,扎河坝方辉橄榄岩绢石化斜方辉石内及颗粒间有橄榄石出熔(图4a),二辉橄榄岩内单斜辉石边部被后期新生的橄榄石交代呈反应边结构(图4g),发生过熔融残余的透辉石边部在后期生成众多橄榄石及新生的单斜辉石、橄榄石叠加在斜方辉石上或沿斜方辉石边部及楔形裂缝生长(图4c,f)。可见,扎河坝橄榄岩存在熔-岩反应的结构标志和反应的新生矿物,也说明熔融亏损的橄榄岩在后期发生过熔-岩反应而产生了再富集作用(Saal et al., 2001; V Le Roux et al., 2007),但缺少熔(流)体渗透(Becker et al., 2001; Seyler et al., 2007; 张宏福, 2008; 罗照华等, 2019)、熔-岩反应的大规模宏观标志(Rampone et al., 2008; Basch et al., 2018),这在一定程度上可能局限了熔岩反应的程度和扎河坝铬铁矿的矿床规模。

7.3 铬铁矿成分差异与蛇绿岩形成的构造背景

蛇绿岩铬铁矿中Cr[#]、Mg[#]和Al₂O₃含量能够反映其形成的岩浆的熔融程度、形成压力和构造背景(Dick and Bullen, 1984; Arai, 1992; Zhou and Robinson, 1994; Pearce et al., 2000),也是判别铬铁矿成因类型的关键指标。如富Al-低Cr(Cr[#]<60)的铬铁矿一般形成于洋中脊或弧后盆地背景中,即MORB型,而俯冲带背景形成富Cr(Cr[#]>60)尖晶石铬铁矿,即SSZ型(Zhou and Robinson, 1994; Uysal et al., 2005, 2009; Akmaz et al., 2014; Ahmed and Abdelmonem, 2015; Erdi et al., 2017)。然而, Zhou et al.(2014)提出,高Cr和高Al铬铁岩可以形成在同一个蛇绿岩内,铬铁矿组成与构造背景的简单对应关系似乎并不存在,因为很多铬铁矿(如罗布莎和阿曼)显示两阶段演化过程(Zhou et al., 2005; Rollinson and Adetunji, 2013; 熊发挥等, 2014, 2015),即原始形成于MOR环境,进而被SSZ熔融改造。事

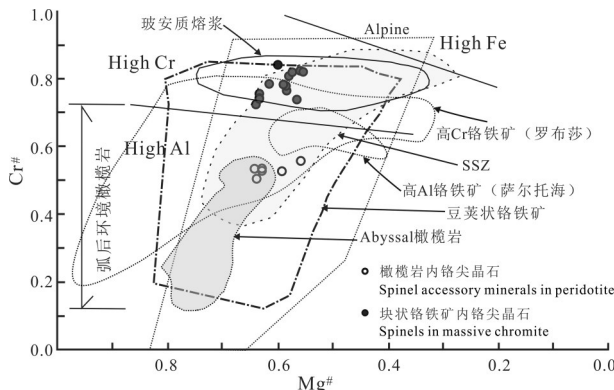


图8 橄榄岩内尖晶石副矿物、块状铬铁矿尖晶石 $\text{Cr}^{\#}$ – $\text{Mg}^{\#}$
($\text{Mg}/(\text{Mg}+\text{Fe}^{2+})$)关系图解

High Cr, High Al 和 High Fe 数据范围引自 Zhou and Bai (1992); 豆英状铬铁矿、层状铬铁矿和 Alpine 型范围参考 Irvine (1967) 和 Leblanc and Nicolas (1992); 玻安质熔浆范围参考 Arai (1992), abyssal 橄榄岩范围参考 Dick and Bullen (1984); 弧后环境橄榄岩范围参考 Monnier et al. (1995), SSZ 环境橄榄岩范围参考 Choi et al. (2008), 萨尔托海铬铁矿数据引自 Zhou et al., 2014; 罗布莎铬铁矿数据引自周二斌等 (2011)

Fig.8 $\text{Cr}^{\#}$ versus $\text{Mg}^{\#}$ ($\text{Mg}/(\text{Mg}+\text{Fe}^{2+})$) diagram of spinels in peridotite and massive chromite

Compositional fields of High Cr, High Al and High Fe are from Zhou and Bai (1992); The podiform, stratiform fields and Alpine-type field are from Irvine (1967) and Leblanc and Nicolas (1992); The boninite field is from Arai (1992). The abyssal peridotite field is from Dick and Bullen (1984); Back-arc Peridotite field is from Monnier et al. (1995); SSZ peridotite field is from Choi et al. (2008); Compositional fields of Sartohay (Zhou et al., 2014); Compositional fields of Luobusha (Zhou E B et al., 2011)

实际上,SSZ背景因富含俯冲板片带来的流体/水(Dick and Bullen, 1984),容易发生高程度部分熔融和充分的熔–岩反应,从而形成大规模铬铁矿(Zhou and Robinson, 1994; Zhou et al., 1996; Arai and Yurimoto, 1994; Arai, 1997; Arai and Matsukage, 1998)。

上述铬铁矿 $\text{Cr}^{\#}$ 值、 Al_2O_3 含量差异及构造背景的对应关系也可能与地幔橄榄岩部分熔融程度有关系(Duke, 1982; Dick and Bullen, 1984):即成熟弧后盆地或洋中脊背景形成的富Al–低Cr型铬铁岩与洋中脊快速扩张、低程度部分熔融形成的拉斑质熔浆有关(Uysal et al., 2009; Ahmed and Abdelmonem, 2015),而SSZ背景形成富 $\text{Cr}^{\#}$ 、低Al铬铁矿是高程度部分熔融的结果, $\text{Cr}^{\#}$ 随地幔岩熔融程度的增高而增高。

同时,参与熔–岩反应物质成分、类型的差异也会造成铬铁矿 $\text{Cr}^{\#}$ 值、 Al_2O_3 含量差异。如:富含 MgO

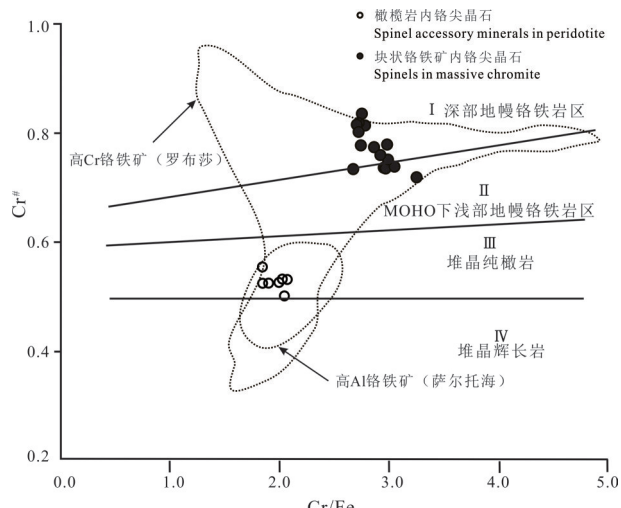


图9 橄榄岩内尖晶石副矿物、块状铬铁矿尖晶石
 Cr/Fe – $\text{Cr}^{\#}$ 关系图解

分区范围参考 Rammlmair (1986), Günay and Çolakoğlu (2016), 萨尔托海铬铁矿数据引自 Zhou et al., (2014); 罗布莎铬铁矿数据引自周二斌等(2011)

Fig.9 $\text{Cr}^{\#}$ versus Cr/Fe diagram of spinels in peridotite and massive chromite

Compositional fields are from Rammlmair (1986), Günay and Çolakoğlu (2016), Compositional fields of Sartohay Zhou et al. (2014); Compositional fields of Luobusha (Zhou E B et al., 2011)

的玻安质熔浆与亏损的方辉橄榄岩反应可形成高Cr型铬铁矿(Zhou and Robinson, 1994, 1997; Zhou et al., 2001; Ahmed and Abdelmonem, 2015),低 MgO 的拉斑玄武质熔体与橄长岩反应(Zhou et al., 2001; 田亚洲和杨经绥, 2016),或熔体与古老大陆岩石圈地幔反应(史仁灯等, 2012; Shi et al., 2012),可形成高 Al_2O_3 、低Cr型铬铁矿。

岛弧的发育程度也是决定 $\text{Cr}^{\#}$ 值、 Al_2O_3 含量的因素,如 Mohamed and Shoji (2017)认为岛弧发育初始阶段的弧前扩张中心形成的铬铁岩具有较高的 Al_2O_3 含量,而成熟岛弧阶段俯冲晚期玻安质熔浆具有更高的 $\text{Cr}^{\#}$ 值。

此外,“地幔对流循环”过程(Foley, 2011; Miura et al., 2012; Ahmed, 2013; Ahmed and Abdelmonem, 2015)不仅使铬铁矿 $\text{Cr}^{\#}$ 值、 $\text{Mg}^{\#}$ 值、 Al_2O_3 含量发生改变,引起的不同类型的地幔岩(SSZ型、MOR型)的共存和叠置,同时洋壳俯冲作为这种循环的重要过程,使得原始橄榄岩–铬铁矿俯冲进入地幔深部以再循环的方式再次出现在原来洋中脊的位置,进而完成循环过程(Arai, 2010; Arai, 2013; 熊发挥等,

2014, 2015; Ahmed and Abdelmonem, 2015; Arai and Miura, 2016)。在后期碰撞造山和蛇绿岩就位后, 形成高Cr和高Al铬铁矿共存于同一个蛇绿岩内 (Roberts, 1988; Zhou and Robinson, 1997; Uysal et al., 2009)。

7.4 扎河坝橄榄岩形成及铬铁矿富集、成矿

古亚洲洋(扎河坝—阿尔曼泰小洋盆)拉张实现了壳幔分异和铬铁矿预富集: 即由于晚寒武世以前发生扎河坝—阿尔曼泰小洋盆开裂, 压力的降低和减压熔融引起深部地幔物质上涌, 形成地幔残留橄榄岩, 熔出大洋玄武岩的同时, 形成副矿物铬尖晶石, 从而使得铬铁矿得以初始富集(图10a)。

随着扎河坝—阿尔曼泰小洋盆洋壳俯冲殆尽和卡拉麦里小洋盆打开、俯冲(李锦铁, 1995), 俯冲带上盘(SSZ)富含俯冲板片带来的流体(Dick and Bullen, 1984; Roberts and Neary, 1993)使浅的地幔楔发生变质作用, 引发方辉橄榄岩发生高程度部分熔融和充分的熔—岩反应(Zhou et al., 2005), 俯冲板片物质的混染可以使地幔岩浆相对富硅和Cr饱和(Zhou et al., 2014)。地幔对流循环使早期MORB背景下形成的铬铁矿进一步聚集形成规模较大的致密块状铬铁矿(图10b)。

8 结 论

(1) 扎河坝二辉橄榄岩内铬尖晶石副矿物具有较低的 Cr_2O_3 、 $\text{Cr}^{\#}$ 和更高的 Al_2O_3 、 MgO 和 $\text{Mg}^{\#}$, 属高Al型, 橄榄岩形成于扎河坝洋扩张环境, 扎河坝块状铬铁矿属SSZ背景高Cr型铬铁矿。

(2) 二辉橄榄岩单斜辉石具有熔融残余结构和熔—岩反应结构, 斜方辉石保留绢石化假晶和部分未蚀变的辉石残余体, 铬尖晶石副矿物具有熔蚀特征。单斜辉石的熔融残余结构是含铬矿物熔融、释放铬的一种表现, 但对富Cr型铬铁矿的形成贡献有限。

(3) 橄榄岩存在熔—岩反应的新生单斜辉石、橄榄石及结构标志。可能存在熔体、流体流与方辉橄榄岩、二辉橄榄岩之间的反应。

(4) 铬铁矿 $\text{Cr}^{\#}$ 值、 Al_2O_3 含量差异可能受地幔橄榄岩部分熔融程度、参与熔—岩反应物质成分及类型的差异、岛弧的发育程度、“地幔对流循环”过程的影响。

(5) 卡拉麦里洋壳俯冲和地幔对流循环使扎河坝早期形成于MORB环境的富Al铬尖晶石富集, 形

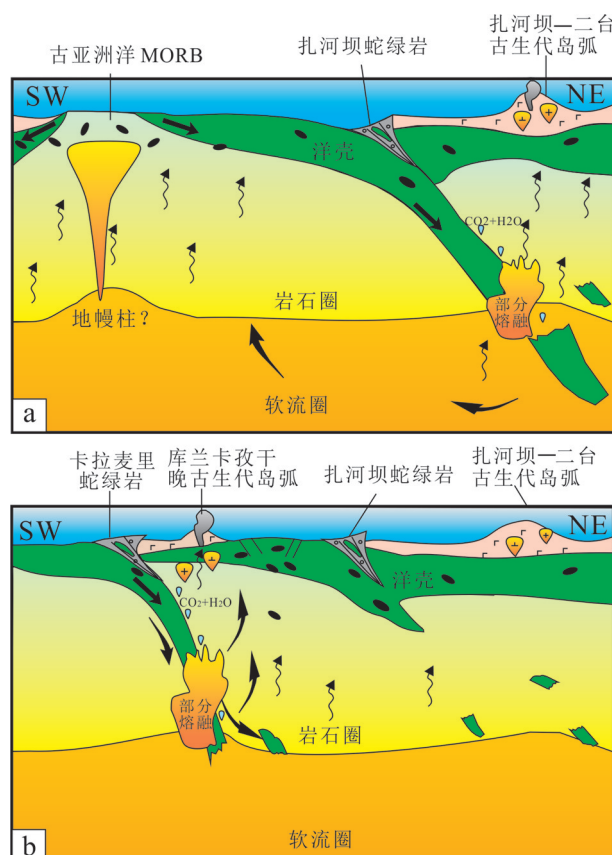


图10 扎河坝蛇绿岩及铬铁矿形成演化示意图
a—扎河坝—阿尔曼泰洋拉张, 地幔上涌, 形成地幔橄榄岩, 铬铁矿预富集, 扎河坝洋洋壳俯冲;b—卡拉麦里洋洋壳俯冲, 地幔对流循环和俯冲带上盘块状铬铁矿形成

Fig.10 Schematic illustration showing

formation and evolution of Zhaheba ophiolite and chromite
a— Stretching of Zhaheba—Aermantai ocean, followed by mantle upwelling, forming of mantle peridotite, chromite preenrichment, and subduction of Zhaheba Oceanic; b— Subduction of Karamaili ocean, accompanied by mantle convection and recycling, forming of massive chromite in supra—subduction zone (SSZ)

成高Cr块状铬铁矿。

注释

①新疆地质矿产局. 2012. 富蕴县幅(L45C002004)1:250000地质调查报告[R].

References

- Ahmed A H, Shoji A, Attia A K. 2001. Petrological characteristics of podiform chromitites and associated peridotites of the Pan African ophiolite complexes of Egypt[J]. Mineralium Deposita, 36: 72–84.
 Ahmed A H. 2013. Highly depleted harzburgite–dunite–chromitite complexes from the Neoproterozoic ophiolite, south Eastern

- Desert, Egypt: A possible recycled upper mantle lithosphere [J]. *Precambrian Research*, 233: 173–192.
- Ahmed A H, Habtoor A. 2015. Heterogeneously depleted Precambrian lithosphere deduced from mantle peridotites and associated chromitite deposits of Al'Ays ophiolite, Northwestern Arabian Shield, Saudi Arabia[J]. *Ore Geology Reviews*, 67: 279–296.
- Akmez R M, Uysalı S, Saka S. 2014. Compositional variations of chromite and solid inclusions in ophiolitic chromitites from the southeastern Turkey: Implications for chromitite genesis[J]. *Ore Geology Reviews*, 58: 208–224.
- Arai S. 1992. Chemistry of chromian spinel in volcanic rocks as a potential guide to magma chemistry[J]. *Mineralogical Magazine*, 56: 173–184.
- Arai S, Yurimoto H. 1994. Podiform chromitites of the Tari–Misaka ultramafic complex, Southwest Japan, as mantle–melt interaction products[J]. *Economic Geology*, 89: 1279–1288.
- Arai S. 1997. Control of wall–rock composition on the formation of podiform chromitites as a result of magma/peridotite interaction[J]. *Resource Geology*, 47(4): 177–187.
- Arai S, Matsukage K. 1998. Petrology of a chromitite micropod from Hess Deep, equatorial Pacific: A comparison between abyssal and alpine-type podiform chromitites[J]. *Lithos*, 43: 1–14.
- Arai S. 2010. Possible recycled origin for ultrahigh-pressure chromitites in ophiolites[J]. *Journal of Mineralogical and Petrological Science*, 105(5): 280–285.
- Arai S. 2013. Conversion of low-pressure chromitites to ultrahigh-pressure chromitites by deep recycling: A good inference[J]. *Earth and Planetary Science Letters*, 379: 81–87.
- Arai S, Miura M. 2016. Formation and modification of chromitites in the mantle[J]. *Lithos*, 264: 277–295.
- Bao Peisheng. 2009. Further discussion on the genesis of the podiform chromite deposits in the ophiolites—questioning about the rock/melt interaction metallogeny[J]. *Geological Bulletin of China*, 28 (12): 1741–1761 (in Chinese with English abstract).
- Barnes S J. 2000. Chromite in komatiites. II. Modification during greenschist to mid–amphibolite facies metamorphism[J]. *Journal of Petrology*, 41: 387–409.
- Barnes S J, Roeder P L. 2001. The range of spinel compositions in terrestrial mafic and ultramafic rocks[J]. *Journal of Petrology*, 42: 2279–2302.
- Basch V, Rampone E, Crispini L, Ferrando C, Ildefonse B, Godard M. 2018. From mantle peridotites to hybrid troctolites: Textural and chemical evolution during melt–rock interaction history (Mt. Maggiore, Corsica, France) [J]. *Lithos*, 323: 4–23.
- Becker H, Shirey S B, Carlson R W. 2001. Effects of melt percolation on the Re–Os systematics of peridotites from a Paleozoic convergent plate margin[J]. *Earth and Planetary Science Letters*, 188: 107–121.
- Bonavia F F, Diella V, Ferrario A. 1993. Precambrian podiform chromitites from Kenticha Hill, Southern Ethiopia[J]. *Economic Geology*, 88: 198–202.
- Choi S H, Shervais J W, Mukasa S B. 2008. Supra–subduction and abyssalmantle peridotites of the coast range ophiolite, California[J]. *Contributions to Mineralogy and Petrology*, 156: 551–576.
- Daniele B, Monique S, Anna C, Luisa O, Enrico B. 2006. Discontinuous melt extraction and weak refertilization of mantle peridotites at the vema Lithospheric Section (Mid–Atlantic Ridge)[J]. *Journal of Petrology*, 47: 745–771.
- Dick H J B, Bullen T. 1984. Chromian spinel as a petrogenetic indicator in abyssal and Alpine–type peridotites and spatially associated lavas[J]. *Contributions to Mineralogy and Petrology*, 86: 54–76.
- Duke J M. 1982. Ore deposit model 7: Magma segregation deposits of chromite[J]. *Geochimica et Cosmochimica Acta*, 39: 1061–1074.
- Elthon D. 1992. Chemical trends in abyssal peridotites: Refertilization of depleted suboceanic mantle[J]. *Journal of Geophysical Research*, 97: 9015–9025.
- Eric H, Snow J E, Peter H, Hofmann A W. 2002. Garnet–field melting and late–stage refertilization in ‘residual’ abyssal peridotites from the Central Indian Ridge[J]. *Journal of Petrology*, 43: 2305–2338.
- Erdi A, İbrahim U, Recep M A, Samet S. 2017. Ophiolitic chromitites from the Kızılıksek area of the Pozanti–Karsanti ophiolite (Adana, southernTurkey): Implication for crystallization from a fractionated boninitic melt[J]. *Ore Geology Reviews*, 90: 166–183.
- Evans B, Frost R B. 1975. Chrome spinel in progressive metamorphism: A preliminary analysis[J]. *Geochimica et Cosmochimica Acta*, 39: 959–972.
- Foley S F. 2011. A reappraisal of redox melting in the earth’s mantle as a function of tectonic setting and time[J]. *Journal of Petrology*, 52: 1363–1391.
- Gonzalez J J M, Proenza J A, Gervilla F, Melgarejo J C, Blanco M J A, Ruiz S R, Griffin W L. 2011. High–Cr and high–Al chromitites from the Sagua de Tanamo district, Mayari–Cristal ophiolitic massif (eastern Cuba): Constraints on their origin from mineralogy and geochemistry of chromian spinel and platinum–group elements[J]. *Lithos*, 125: 101–121.
- Günay K, Colakoğlu A R. 2016. Spinel compositions of mantle–hosted chromitite from the Eastern Anatolian ophiolite body, Turkey: Implications for deep and shallow magmatic processes[J]. *Ore Geology Reviews*, 73: 29–41.
- Hao Ziquo. 1991. Study on the genesis of ophiolites and podiform chromite deposits of the western Junggar area, Xinjiang[J]. *Bulletin of the Chinese Academy of Geological Sciences*, 23: 73–83(in Chinese with English abstract).
- He Guoqi, Li Maosong, Jia Jindou, Zhou Hui. 2001. A discussion on age and tectonic significance of ophiolite in Eastern Junggar, Xinjiang[J]. *Acta Scientiarum Naturalium Universitatis Pekinensis*, 37(6): 852–858(in Chinese with English abstract).
- Huang Qishuai, Shi Rendeng, Ding Binghua, Liu Deliang, Zhang Xiaoran, Fan Shuaiquan, Zhi Xiachen. 2012. Re–Os isotopic evidence of MOR–type ophiolite from the Bangong Co for the

- opening of Bangong–Nu Jiang Tethys Ocean[J]. *Acta Petrologica et Mineralogica*, 31(4): 465–478 (in Chinese with English abstract).
- Irvine T N. 1967. Chromium spinels as a petrogenetic indicator petrologic applications[J]. *Canadian Journal of Earth Sciences*, 11 (4): 71–103.
- Jian Ping, Liu Dunyi, Zhang Qi, Zhang Fuqin, Shi Yuruo, Shi Guanghai, Zhang Luqiao, Tao Hua. 2003. Shrimp dating of ophiolite and leucocratic rocks within ophiolite[J]. *Earth Science Frontiers*, 11 (4): 71–103 (in Chinese with English abstract).
- Kamenetsky V S, Crawford A J, Meffre S. 2001. Factors controlling chemistry of magmatic spinel: An empirical study of associated olivine, Cr–spinel and melt inclusions from primitive rocks[J]. *Journal of Petrology*, 42: 655–671.
- Li D, He D F, Santosh M, Tang J Y. 2014. Petrogenesis of Late Paleozoic volcanics from the Zhaheba depression, East Junggar: Insights into collisional event in an accretionary orogen of Central Asia[J]. *Lithos*, 184–187, 167–193.
- Luo J, Xiao W J, Wakabayashi W, Han C M, Zhang J E, Wan B, Ao S J, Zhang Z Y, Tian Z H, Song D F, Chen Y C. 2017. The Zhaheba ophiolite complex in Eastern Junggar (NW China): Long lived supra–subduction zone ocean crust formation and its implications for the tectonic evolution in southern Altaiids[J]. *Gondwana Research*, 43: 17–40.
- Leblanc M, Nicolas A. 1992. Ophiolitic chromitites[J]. *International Geology Review*, 34: 653–686.
- Li Jinyi. 1991. Early Paleozoic evolution of lithosphere plate, east Junggar, Xinjiang[J]. *Bulletin of the Chinese Academy of Geological Sciences*, 23: 1–12 (in Chinese with English abstract).
- Li Jinyi. 1995. Main characteristics and emplacement processes of the east Junggar ophiolites, Xinjiang, China[J]. *Acta Petrologica Sinica*, 11(Supp.): 37–84 (in Chinese with English abstract).
- Li Rongshe, Ji Wenhua, Xiao Peixi, Ma Zhongping, Cheng Junlu, Pan Shujuan. 2012. The periodical achievement and new cognitions of regional geological survey, northern Xinjiang[J]. *Xinjiang Geology*, 30(3): 253–257 (in Chinese with English abstract).
- Liu Ting, Zheng Youye, Wang Pengchong, Yang Weiguang, Guo Tongjun. 2019. Geochemical indicator for podiform chromite mineralization and its formation mechanism[J]. *Bulletin of Mineralogy, Petrology and Geochemistry*, 38(1): 176–194 (in Chinese with English abstract).
- Liu Wei, Zhang Xiangbing. 1993. The characteristics and geological significance of Ulungur–Zhaisangpo tectonic setting[C]// Tu Guangchi(ed.). *New Progress of Solid Geosciences in Northern Xinjiang*. Beijing: Science Press, 217–228 (in Chinese with English abstract).
- Luo Zhaohua, Jiang Xumin, Liu Xiao, Li Zhong, Wu Zongchang, Jing Wenchoao. 2019. Imprints of fluid process of shell dunite in ophiolitic chromite deposits: Evidences from geology, petrology and crystal chemistry of olivine found in Luobusha and Zedang ophiolites in the Yarlung Zangbo suture zone, Tibet[J]. *Earth Science Frontiers*, 26 (1): 272–285 (in Chinese with English abstract).
- Melcher F, Grum W, Thalhammer T V, Thalhammer O A R. 1999. The giant chromite deposits at Kempirsai, Urals: Constraints from trace element (PGE, REE) and isotope data[J]. *Mineralium Deposita*, 34: 250–272.
- Miura M, Arai S, Ahmed A H, Mizukami T, Okuno M, Yamamoto S. 2012. Podiform chromitite classification revisited: A comparison of discordant and concordant chromitite pods from Wadi Hilti, northern Oman ophiolite [J]. *Journal of Asian Earth Sciences*, 59: 52–61.
- Mohamed Z K, Shoji A. 2017. Peridotite–chromitite complexes in the Eastern Desert of Egypt: Insight into Neoproterozoic sub–arc mantle processes [J]. *Gondwana Research*, 52: 59–79.
- Monnier C, Girardeau J, Maury R, Cotten J. 1995. Back–arc basin origin for the East Su–lawesi ophiolite (eastern Indonesia) [J]. *Geology*, 23: 851–854.
- Niu Heicai, Shan Qiang, Zhang Haixiang, Yu Xueyuan. 2007. $^{40}\text{Ar}/^{39}\text{Ar}$ geochronology of the ultrahigh–pressure metamorphic quartz–magnesite in Zhaheba, eastern Junggar, Xinjiang[J]. *Acta Petrologica Sinica*, 23(7): 1627–1634 (in Chinese with English abstract).
- Pan Chengze, Qiu Lin, Ye Xiantao, Dong Yongguan. 2016. Zircon U–Pb ages and Hf–O isotope compositions of the Zhaheba ophiolite in the northern margin of the Junggar terrane and their tectonic implications[J]. *East China Geology*, 37(2): 106–112 (in Chinese with English abstract).
- Pearce J A, Barker P F, Edwards S J, Parkinson I J, Leat P T. 2000. Geochemistry and tectonic significance of peridotites from the South Sandwich arc basin system, south Atlantic[J]. *Contributions to Mineralogy and Petrology*, 139: 36–53.
- Rammler D. 1986. Chromite in Philippines: Its relationship to the tectonic setting of the host ophiolites: Examples from Zambales and Palawan, in Chromites. UNESCO's IGCP–197 Project Metallogeny of Ophiolites: Athens, Greece, Theopastus 199–228.
- Rampone E, Piccardo G B, Hofmann A W. 2008. Multi–stage melt–rock interaction in the Mt. Maggiore (Corsica, France) ophiolitic peridotites: Microstructural and geochemical evidence [J]. *Contributions to Mineralogy and Petrology*, 156: 453–475.
- Roberts S. 1988. Ophiolitic chromitite formation: A marginal basin phenomenon? [J]. *Economic Geology*, 83: 1034–1036.
- Roberts S, Neary C R. 1993. Petrogenesis of ophiolitic chromitites[C]// Prichard H M, Alabaster T, Harris N B W, Neary C R (eds.). *Magmatic Processes and Plate Tectonics*. Geological Society London Special Publications, 76(1): 257–272.
- Rollinson H, Adetunji J. 2013. Mantle podiform chromitites do not form beneath mid–ocean ridges: A case study from the Moho transition zone of the Oman ophiolite[J]. *Lithos*, 177: 314–327.
- Saal A E, Takazawa E, Frey F A, Shimizu N, Hart S R. 2001. Re–Os Isotopes in the Horoman Peridotite: Evidence for Refertilization? [J]. *Journal of Petrology*, 42(1): 25–37.
- Seyler M, Toplis M J, Lorand J P, Luguet A, Cannat M. 2001. Clinopyroxene microtextures reveal incompletely extracted melts

- in abyssal peridotites[J]. *Geology*, 29: 155–158.
- Seyler M, Lorand J P, Dick H J B, Drouin M. 2007. Pervasive melt percolation reactions in ultra-depleted refractory harzburgites at the Mid-Atlantic Ridge, 15 degrees 20' N: ODP Hole 1274A[J]. *Contributions to Mineralogy and Petrology*, 153: 303–319.
- Shi R, Griffin W L, Reilly S Y O, Zhou M, Zhao G, Huang Q, Zhang X, Ding B, Ding L. 2012. Archean mantle contributes to the genesis of chromitite in the Palaeozoic Sartohay ophiolite, Asiatic Orogenic Belt, northwestern China [J]. *Precambrian Research*, 216–219: 87–94.
- Shi Rendeng, Huang Qishuai, Liu Deliang, Fan Shuaiquan, Zhang Xiaoran, Ding Lin, William L Griffin, Suzanne Y O'Reilly. 2012. Recycling of ancient subcontinental lithospheric mantle constraints on the genesis of the ophiolitic podiform chromitites[J]. *Geological Review*, 58(4): 643–652(in Chinese with English abstract).
- Su Benxun, Bai Yang, Chen Chen, Liu Xai, Xiao Yan, Tang Dongmei, Liang Zi, Cui Mengmeng, Peng Qingshan. 2018. Petrological and mineralogical investigations on hydrous properties of parental magmas of chromite deposits[J]. *Bulletin of Mineralogy, Petrology and Geochemistry*, 37(6): 1035–1046 (in Chinese with English abstract).
- Su B X, Zhou M F, Jing J J, Robinson P T, Chen C, Xiao Y, Liu X, Shi R D, Lennaz D, Hu Y. 2019. Distinctive melt activity and chromite mineralization in Luobusa and Purang ophiolites, southern Tibet: Constraints from trace element compositions of chromite and olivine[J]. *Chinese Science Bulletin*, 64: 108–121.
- Tian Yazhou, Yang Jingsui. 2016. Study on the mineral inclusions in Sartohay chromitites[J]. *Acta Geologica Sinica*, 90(11): 3114–3128 (in Chinese with English abstract).
- Trevor J F, David H G, Leonid V D, Andrew W M. 2008. The composition of near-solidus partial melts of fertile peridotite at 1 and 1.5 GPa: Implications for the petrogenesis of MORB[J]. *Journal of Petrology*, 49: 591–613.
- Uysal İ, Zaccarini F, Garuti G, Meisel T, Tarkian M, Bernhardt H J, Sadiklar M B. 2007. Ophiolitic chromitites from the Kahramanmaraş area, southeastern Turkey: Their platinum group elements (PGE) geochemistry, mineralogy and Os isotope signature[J]. *Ofioliti*, 32: 151–161.
- Uysal İ, Sadiklar M B, Tarkian M, Karslı O, Aydin F. 2005. Mineralogy and composition of the chromitites and their platinum-group minerals from Ortaca (Mugla–SW Turkey): Evidence for ophiolitic chromitite genesis[J]. *Mineral. Petrol.*, 83: 219–242.
- Uysal İ, Tarkian M, Sadiklar M B, Zaccarini F, Meisel T, Garuti G, Heidrich, S. 2009. Petrology of Al- and Cr-rich ophiolitic chromitites from the Muğla, SW Turkey: Implications from composition of chromite, solid inclusions of platinum-group mineral(PGM), silicate, and base-metal mineral(BMM), and Os-isotope geochemistry[J]. *Contributions to Mineralogy and Petrology*, 158: 659–674.
- V Le Roux, J L Bodinier, A Tommasi, O Alard, J M Dautria, A Vauchez, A J V Riches. 2007. The Lherz spinel lherzolite: Refertilized rather than pristine mantle [J]. *Earth and Planetary Science Letters*, 259: 599–612.
- Wang Xibin, Bao Peisheng. 1987. The genesis of podiform chromite deposits—a case study of the Luobusa chromite deposit, Tibet[J]. *Acta Geologica Sinica*, (2): 166–181 (in Chinese with English abstract).
- Xiao W J, Windley B F, Badarch G, Sun S, Li J, Qin K, Wang Z. 2004. Palaeozoic accretionary and convergent tectonics of the southern Altaiids: Implications for the growth of Central Asia[J]. *Journal of the Geological Society, London*, 161: 339–342.
- Xiao W J, Windley B F, Yuan C, Sun M, Han C M, Lin S F, Chen H L, Yan Q R, Liu D Y, Qin K Z, Li J L, Sun S. 2009. Paleozoic multiple subduction accretion processes of the southern Altaiids[J]. *American Journal of Science*, 309: 221–270.
- Xiao Xuchang, Tang Yaoqing. 1991. *Tectonic Evolution of the Southern Margin of the Paleo-Asian Composite Megasuture Zone*[M]. Beijing: Beijing Science and Technology Press, 1–150 (in Chinese with English abstract).
- Xiong Fahui, Yang Jingsui, Liu Zhao. 2013. Multi-stage formation of the podiform chromite[J]. *Geology in China*, 40(3): 820–839 (in Chinese with English abstract).
- Xiong Fahui, Yang Jingsui, Ba Dengzhu, Liu Zhao, Xu Xiangzhen, Feng Gaungying, Niu Xiaolu, Xu Jifeng. 2014. Different type of chromitite and genetic model from Luobusa ophiolite, Tibet[J]. *Acta Petrologica Sinica*, 30(8): 2137–2163 (in Chinese with English abstract).
- Xiong Fahui, Yang Jingsui, Xu Xiangzhen, Lai Shenming, Zhang Lan, Guo Guoling, Chen Yanhong, Zhao Hui. 2015. The prospects of chromitite in ophiolite of Yarlung Zangbo Suture Zone, Tibet[J]. *Geology in China*, 42(5): 1535–1558 (in Chinese with English abstract).
- Zaccarini F, Garuti G, Proenza J A, Campos L, Thalhammer O A R, Aiglsperger T, Lewis J. 2011. Chromite and platinum-group-elements mineralization in the Santa Elena ophiolitic ultramafic nappe (Costa Rica): Geodynamic implications[J]. *Geologica Acta*, 9: 407–423.
- Zhang Hongfu. 2008. Variation of Re–Os isotopic system during peridotite–melt interaction: Implication for the meaning of Re–Os isotopic age of Cenozoic mantal peridotites from the North China craton[J]. *Acta Petrologica Sinica*, 24(11): 2457–2467 (in Chinese with English abstract).
- Zhang Yuanyuan, Guo Zhaojie. 2010. New constraints on formation ages of ophiolites in northern Junggar and comparative study on their connection[J]. *Acta Petrologica Sinica*, 26(2): 421–430 (in Chinese with English abstract).
- Zeng L J, Niu H C, Bao Z W, Shan Q, Li H, Li N B, Yang W B. 2015. Petrogenesis and tectonic significance of the plagiogranites in the Zhaheba ophiolite, Eastern Junggar orogen, Xinjiang, China[J]. *Journal of Asian Earth Sciences*, 113: 137–150.
- Zhou Erbin, Yang Zhushen, Jiang Wan, Hou Zengqian, Guo Fusheng, Hong Jun. 2011. Study on mineralogy of Cr-spinel and genesis of Luobusa chromite deposit in South Tibet[J]. *Acta Petrologica Sinica*, 27(7): 2060–2072 (in Chinese with English abstract).

- Zhou M F, Bai W J. 1992. Chromite deposits in China and their origin[J]. Mineralium Deposita, 27: 192–199.
- Zhou Meifu, Bai Wenji. 1994. The origin of the podiform chromite deposits[J]. Mineral Deposits, 13(3): 242–249(in Chinese with English abstract).
- Zhou M F, Robinson P T. 1994. High-chromium and high-aluminium podiform chromitites, Western China, relationship to partial melting and melt/rock interaction in the upper mantle[J]. International Geology Review, 36: 678–686.
- Zhou M F, Robinson P T, Malpas J, Li Z. 1996. Podiform chromitites from the Luobusa ophiolite (southern Tibet): Implications for melt–rock interaction and chromite segregation[J]. Journal of Petrology, 37: 3–21.
- Zhou M F, Robinson P T. 1997. Origin and tectonic environment of podiform chromite deposits[J]. Economic Geology, 92: 259–262.
- Zhou M F, Sun M, Keays R R, Kerrich R. 1998. Controls on the platinum-group elemental distributions in high-Cr and high-Al chromitites: A case study of the podiform chromitites from the Chinese orogenic belts[J]. Geochimica et Cosmochimica Acta, 62: 677–688.
- Zhou M F, Robinson P T, Malpas J, Aitchison J, Sun M, Bai W J, Hu X F, Yang J S. 2001. Melt–mantle interaction and melt evolution in the Sartohay high-Al chromite deposits of the Dalabute ophiolite (NW China) [J]. Journal of Asian Earth Sciences, 19: 517–534.
- Zhou M F, Robinson P T, Malpas J, Edwards S, Qi, L. 2005. REE and PGE geochemical constraints on the formation of dunites in the Luobusha ophiolite, Southern Tibet[J]. Journal of Petrology, 46(3): 615–639.
- Zhou M F, Robinson P T, Su B X, Gao J F, Li J W, Yang J S, Malpas J. 2014. Compositions of chromite, associated minerals, and parental magmas of podiform chromite deposits: The role of slab contamination of asthenospheric melts in suprasubduction zone environments[J]. Gondwana Research, 26: 262–283.
- 李荣社, 计文化, 校培喜, 马中平, 陈隽璐, 潘术娟. 2012. 北疆区域地质调查阶段性成果与新认识[J]. 新疆地质, 30(3): 253–257.
- 刘婷, 郑有业, 王朋冲, 杨伟光, 郭统军. 2019. 豆英状铬铁矿床成矿地球化学指标对比和成矿作用讨论[J]. 矿物岩石地球化学通报, 38(1): 176–194.
- 刘伟, 张湘炳. 1993. 乌伦古–斋桑泊构造杂岩带特征及其地质意义[C]// 涂光炽主编. 新疆北部固体地球科学新进展. 北京: 科学出版社, 217–228.
- 罗照华, 江秀敏, 刘晓, 李重, 吴宗昌, 井文超. 2019. 蛇绿岩型铬铁矿床壳纯橄榄岩中的流体过程印记: 来自西藏雅鲁藏布江缝合带罗布莎和泽当岩体的地质学、岩石学和橄榄石晶体化学证据[J]. 地学前缘, 26(1): 272–285.
- 牛贺才, 单强, 张海祥, 于学元. 2007. 东准噶尔扎河坝超高压变质成因石英镁岩的 $^{40}\text{Ar}/^{39}\text{Ar}$ 同位素年代学信息及地质意义[J]. 岩石学报, 23(7): 1627–1634.
- 潘成泽, 邱林, 叶现韬, 董永观. 2016. 扎河坝蛇绿岩锆石 U-Pb 年龄、Hf-O 同位素组成及其地质意义[J]. 华东地质, 37(2): 106–112.
- 史仁灯, 黄启帅, 刘德亮, 樊帅权, 张晓冉, 丁林, William L G, Suzanne Y O'Reilly. 2012. 古老大陆岩石圈地幔再循环与蛇绿岩中铬铁矿床成因[J]. 地质论评, 58(4): 643–652.
- 苏本勋, 白洋, 陈晨, 刘霞, 肖燕, 唐冬梅, 梁子, 崔梦萌, 彭青山. 2018. 铬铁矿床母岩浆含水性的岩石矿物学探讨[J]. 矿物岩石地球化学通报, 37(6): 1035–1046.
- 田亚洲, 杨经绥. 2016. 萨尔托海铬铁矿中的矿物包体研究[J]. 地质学报, 90(11): 3114–3128.
- 王希斌, 鲍佩声. 1987. 豆英状铬铁矿的成因——以西藏自治区罗布莎铬铁矿床为例[J]. 地质学报, (2): 166–181.
- 肖序常, 汤耀庆. 1991. 古中亚复合巨型缝合带南缘构造演化[M]. 北京: 北京科学技术出版社, 1–150.
- 熊发挥, 杨经绥, 刘钊. 2013. 豆英状铬铁矿多阶段形成过程的讨论[J]. 中国地质, 40(3): 820–839.
- 熊发挥, 杨经绥, 巴登珠, 刘钊, 徐向珍, 冯光英, 牛晓露, 许继峰. 2014. 西藏罗布莎不同类型铬铁矿的特征及成因模式讨论[J]. 岩石学报, 30(8): 2137–2163.
- 熊发挥, 杨经绥, 徐向珍, 来盛民, 张岚, 郭国林, 陈艳虹, 赵慧. 2015. 雅鲁藏布江缝合带蛇绿岩中铬铁矿的前景讨论[J]. 中国地质, 42(5): 1535–1558.
- 张宏福. 2008. 橄榄岩–熔体相互作用过程中 Re–Os 体系的变化趋势: 对华北新生代地幔橄榄岩 Re–Os 年龄含义的启示[J]. 岩石学报, 24(11): 2457–2467.
- 张元元, 郭召杰. 2010. 准噶尔北部蛇绿岩形成时限新证据及其东、西准噶尔蛇绿岩的对比研究[J]. 岩石学报, 26: 421–430.
- 周二斌, 杨竹森, 江万, 侯增谦, 郭福生, 洪俊. 2011. 藏南罗布莎铬铁矿床铬尖晶石矿物学与矿床成因研究 [J]. 岩石学报, 27(7): 2060–2072.
- 周美付, 白文吉. 1994. 对豆英状铬铁矿床成因的认识[J]. 矿床地质, 13(3): 242–249.

附中文参考文献

- 鲍佩声. 2009. 再论蛇绿岩中豆英状铬铁矿的成因——质疑岩石/熔体反应成矿说[J]. 地质通报, 28(12): 1742–1761.
- 黄启帅, 史仁灯, 丁炳华, 刘德亮, 张晓冉, 樊帅权, 支霞臣. 2012. 班公湖 MOR 型蛇绿岩 Re–Os 同位素特征对班公湖—怒江特提斯洋裂解时间的制约[J]. 岩石矿物学杂志, 31(4): 465–478.
- 郝梓国. 1991. 新疆西准噶尔地区蛇绿岩与豆英型铬铁矿床的成因研究[J]. 中国地质科学院院报, 23: 73–83.
- 何国琦, 李茂松, 贾进斗, 周辉. 2001. 论新疆东准噶尔蛇绿岩的时代及意义[J]. 北京大学学报(自然科学版), 37(6): 852–858.
- 简平, 刘敦一, 张旗, 张福勤, 石玉若, 施光海, 张履桥, 陶华. 2003. 蛇绿岩及蛇绿岩中淡色岩的 SHRIMP U–Pb 测年[J]. 地学前缘, 10(4): 439–456.
- 李锦轶. 1991. 试论新疆东准噶尔早古生代岩石圈板块构造演化[J]. 中国地质科学院院报, 23(3): 1–12.
- 李锦轶. 1995. 新疆东准噶尔蛇绿岩的基本特征和侵位历史[J]. 岩石学报, 13(3): 242–249.